Photo-responses of Metal-Oxide-Semiconductor Transistors

A dissertation presented to the
Chinese University of Hong Kong
in partial fulfillment of the
requirements for the
degree of Master
of Science
by
K.Y.Tong, B.Sc.(Eng)
1974

SUMMARY

In this project, Metal-Oxide-Semiconductor Transistors (MOST) with semi-transparent gate electrodes were fabricated. The aims were to study the photocurrent in the MOST due to (1) optical transition of carriers between the energy bands in the silicon under the gate, (2) direct optical excitation of Si-SiO_2 interface state carriers into the semiconductor.

The dependence of the photocurrent on the drain and gate voltages at different light intensity was measured for illumination causing interband transition of carriers. Two mechanisms responsible for the photocurrent were found in our samples : (1) diffusion of photogenerated minority carriers from the bulk to the drain, (2) increase of carrier concentration in the channel due to optical injection. Some observed characteristics of the MOST under illumination were discussed.

Monochromatic sub-bandgap light from a globar and spectrometer was used to study the possibility of observing the direct excitation of Si-SiO_2 interface state carriers. The result was so far negative. A simple theory was used to estimate the minimum photon flux density required for observing a photocurrent due to such effects. It was shown that the sensitivity of experiments for observing direct optical excitation of surface states in Si was low because the surface states were in good thermal communication with the energy bands.

List of Symbols

(Symbol with an additional asterisk represents the corresponding quantity under illumination)

A_J junction area (cm^2)

C_i oxide capacitance per unit area ($F\ cm^{-2}$)

c_n thermal capture constant of electrons at a surface state ($cm^3\ sec^{-1}$)

c_p thermal capture constant of holes at a surface state ($cm^3\ sec^{-1}$)

D_p diffusion coefficient of holes ($cm^2\ sec^{-1}$)

E_c the minimum electron energy level in the conduction band

E_{FN} quasi-Fermi levels for electrons

E_{FP} quasi-Fermi levels for holes

E_i Fermi level for the intrinsic material (approx. $(E_c + E_v)/2$)

E_s electric field at the semiconductor surface

E_t energy level of a surface state

E_v the maximum electron energy level in the valence band

e_n thermal emission constant of electrons at a surface state ($cm^3\ sec^{-1}$)

e_p thermal emission constant of holes at a surface state (cm^3 sec)

f occupation probability by electrons at a surface state

Δf change of f with optical excitation of surface states

F photon flux density ($sec^{-1}\ cm^{-2}$)

F_s space charge factor as defined in Eq. 1.15

g_D	drain conductance
g_{DS}	saturation drain conductance
g_m	transconductance
G	optical generation rate of carriers in the bulk($cm^{-3}sec^{-1}$)
G_s	surface generation rate of carriers as calculated from a single surface state (cm^{-2} sec^{-1})
I_D	drain current
I_{DS}	saturation drain current
I_p	increase of the drain current under illumination (photocurrent in MOST)
I_{po}	photocurrent in MOST by diffusion of minority carriers
k	Boltzmann 's constant
L	channel length in MOST (cm)
ΔL	change of L due to the drain voltage after saturation
L_D	intrinsic Debye length (cm)
L_p	diffusion length of holes (cm)
m^*	effective mass of carrier
N_D	density of doped donors in the semiconductor (cm^{-3})
n_i	intrinsic carrier concentration (cm^{-3})
n_o	bulk electron concentration in equilibrium (cm^{-3})
Δn_o	increase of n_0 under illumination (cm^{-3})
n_s	electron concentration at the semiconductor surface (Cm^{-3})
p	hole concentration (cm^{-3})
p_o	bulk hole concentration in equilibrium (cm^{-3})
Δp_o	increase of p_o under illumination (cm^{-3})
p_s	hole concentration at the semiconductor surface (cm^{-3})

q electron charge (1.602×10^{-19} coul.)

Q_B depletion layer charge per unit surface area (Coul. cm^{-2})

Q_p charge in the channel per unit surface area (Coul. cm^{-2})

Q_s charge in the semiconductor surface space charge region (per unit surface area) (Coul. cm^{-2})

Q_{ss} total surface state charge (Coul. cm^{-2})

Q_T charge trapped in the surface states causing a lower effective mobility of holes in the channel (Coul cm^{-2})

r_a rate of thermal capture of electrons at a surface state (sec^{-1} cm^{-2})

r_b rate of thermal emission of electrons at a surface state (sec^{-1} cm^{-2})

r_c rate of thermal capture of holes at a surface state (sec^{-1} cm^{-2})

r_d rate of thermal emission of holes at a surface state (sec^{-1} cm^{-2})

r_e rate of optical excitation of electrons at a surface state (sec^{-1} cm^{-2})

r_f rate of optical excitation of holes at a surface state (sec^{-1} cm^{-2})

T absolute temperature

V_D drain voltage

V_{DS} saturation drain voltage

V_{fb} flatband voltage in MOS

V_G gate voltage

V_T turn-on voltage of MOST

V_{th} thermal velocity of electron (cm sec^{-1})

V_y voltage in the channel of a MOST

u_s normalised surface potential (to $\frac{kT}{q}$ units)

Z width of the channel in MOST (cm)

ψ_B potential between the intrinsic level and the Fermic level in the bulk (volt)

ψ_s surface potential (volt)

$\Delta\psi_s$ surface photovoltage (volt)

ε_s permitivity of SiO_2 (F cm^{-1})

ε_{ox} permitivity of Si (F cm^{-1})

μ_p hole mobility in the bulk (cm^2 $volt^{-1}$ sec^{-1})

μ_p' effective hole mobility in the channel ($cm^2 volt^{-1}$ sec^{-1})

τ lifetime of excess minority carrier (sec)

σ_n thermal capture cross section of electrons at a surface state (cm^2)

σ_p thermal capture cross section of holes at a surface state (cm^2)

σ_n^o optical capture cross section of electrons at a surface state (cm^2)

σ_p^o optical capture cross section of holes at a surface state (cm^2)

$\Delta_n = \frac{\Delta n_o}{n_o}$

$\Delta_p = \frac{\Delta p_o}{p_o}$

$\lambda = \left(\frac{p_o}{n_o}\right)^{\frac{1}{2}}$

α as defined in Eqn. 1.11

Acknowledgement

I should like to express my thanks to Drs. Y.W.Lam, H.L.Kwok for their helpful discussions during the work. I also wish to thank Hitachi for the supply of masks, to staff group of the solid state laboratory, Electronics Department, C.U.H.K. for advice during the fabrication of samples and to Dr. Alfred Leung of the Physics Department, C.U.H.K. for making the spectrometer available.

CONTENTS

I. INTRODUCTION

The operating principle of the Metal-Oxide-Semiconductor-Transistor (MOST) was known even before the advent of bipolar transistors. In 1940's the surface field effect was studied by Shockley and Pearson [1], but the MOST was only successfully fabricated in 1960. The delay reflected the difficulty of obtaining a stable $Si-SiO_2$ interface which greatly affected the properties of the MOST. The basic device characteristics were studied by Ihanotola and Moll [2], Sah [3], Hofstein and Heiman [4].

There have been numerious studies on the electrical properties of the MOST and the related surface physics because it is an useful device with high input impedance and low power consumption. In this work, a MOST with a semi-transparent gate electrode was fabricated and its responses to photons of energies both greater than and below the Silicon bandgap were studied. An introduction to the aims of the project together with some review on related topics are described in the following sections .

1.1 Basic characteristics of the MOST

Fig. 1.1 shows the structure of a P-channel MOST with a N-type substrate and heavily doped P-type source

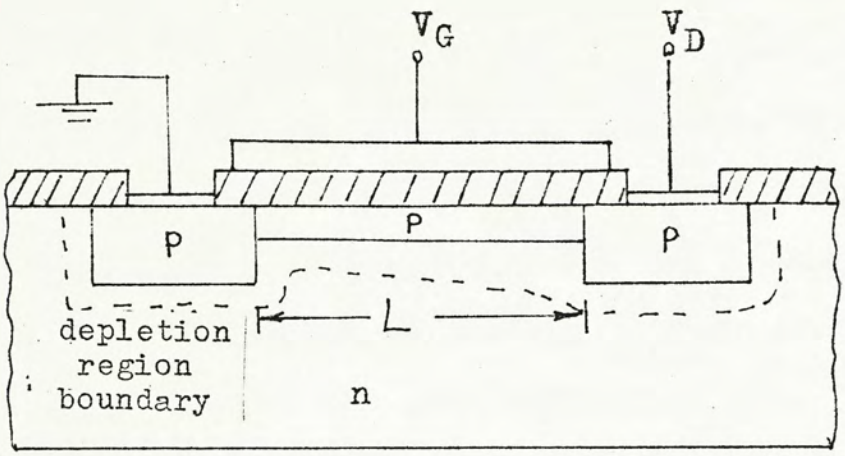

Fig. 1.1 Structure of MOST

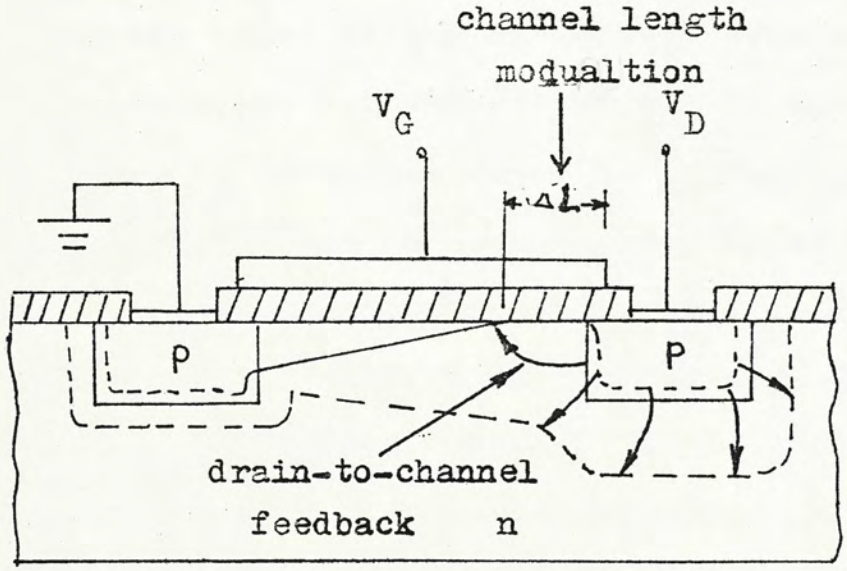

Fig. 1.2 MOST beyond saturation

and drain regions. By applying a voltage to the gate, the surface space charge region between the source and the drain can be inverted, depleted or accumulated. When an inversion layer is formed under the gate, the drain and source are connected by a conducting channel. The charge concentration in the channel and hence the drain current can be directly controlled by the surface electric field through the SiO_2 due to the gate voltage.

The characteristics of the MOST are greatly influenced by the interface states at the Si-SiO_2 interface and the positive ionic charges which are invariably found in the oxide. Due to their presence and the difference in work function between Silicon and the gate electrode, considerable electric field may exist at the Si surface even at zero gate bias. Because the net charges at the Si surface are usually positive, an inversion layer is often induced in a P-type substrate, and an accumulation layer in a N-type substrate. Therefore P-channel devices usually require a minimum negative gate voltage called the turn-on voltage in order to form a conducting channel.

The basic characteristics of the MOST are obtained with the following assumptions:

1. The difference in work function between the gate and the Si substrate, surface states, oxide charges are all represented by a flatband voltage V_{fb} which is the gate voltage required to maintain a flatband in the semiconductor.
2. The mobility of carriers in the inversion layer is constant.
3. The drain current comes only from the channel current. The generation current from the depletion region, channel, and surface states are negligible.
4. Only the drift current of carriers in the channel is considered. Diffusion current can be neglected.
5. There is no leakage current through the oxide.
6. The transverse field E_x in the channel is much larger than the longitudinal field E_y. This is called the gradual channel approach.

In Fig. 1.3 V_y is the voltage in the channel at a distance y from the source. Since V_y is the effective reverse bias between the P-channel and the N-type bulk, the quasi-Fermi levels E_{FP}, E_{FN} are at a separation of qV_y apart and are assumed to be flat within the depletion region. The surface potential ψ_s can be approximated as $V_y - 2\psi_B$ at strong inversion, where ψ_B is the potential between the Fermi level and the intrinsic level in the bulk. The charge per unit surface area in the depletion region $Q_B(y)$ is given by

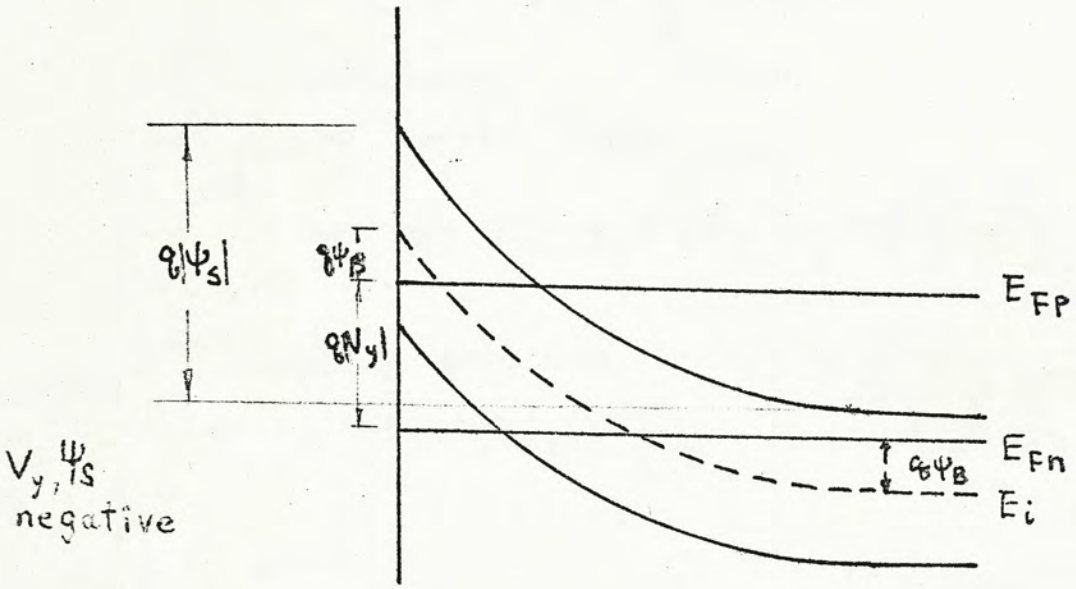

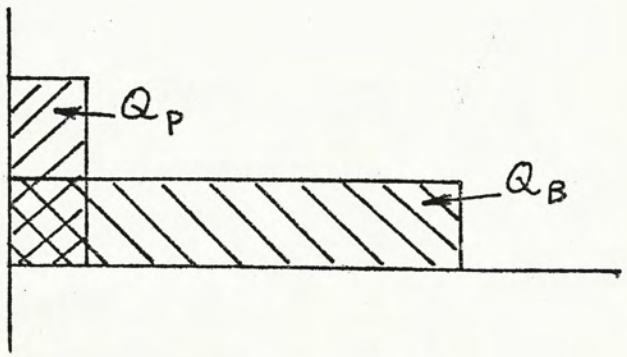

Fig. 13 Energy band diagram of the semiconductor with an inverted channel at distance y from the source

$$Q_B(y) = \sqrt{2\varepsilon_s q N_D(-V_y + 2\psi_B)} \qquad (1.1)$$

The total charge induced in the semiconductor $Q_s(y)$ is given by

$$Q_s(y) = [-V_G + V_{fb} + V_y - 2\psi_B]C_i \qquad (1.2)$$

$\therefore$ the inversion layer charge

$$Q_p(y) = Q_s(y) - Q_B(y)$$

$$= -[V_G - V_{fb} - V_y + 2\psi_B]C_i - \sqrt{2\varepsilon_s q N_D(-V_y + 2\psi_B)} \qquad (1.3)$$

Since the electric field along the channel is $\frac{\partial V_y}{\partial y}$, the drain current $I_D = -q\mu_p' Q_p(y)\frac{\partial V_y}{\partial y}$ (1.4)

Solving Eq. 1,4 gives

$$I_D = \frac{Z}{L}\mu_p' C_i\left\{\left(V_G - V_{fb} + 2\psi_B - \frac{1}{2}V_D\right)V_D + \frac{2}{3}\frac{\sqrt{2\varepsilon_s q N_D}}{C_i}\left[(-V_D + 2\psi_B)^{3/2} - (2\psi_B)^{3/2}\right]\right\} \qquad (1.5)$$

At low drain voltage V_D,

$$I_D \simeq \frac{Z}{L}\mu_p' C_i\left\{(V_G - V_T)V_D - \frac{V_D^2}{2}\right\} \qquad (1.6)$$

where the turn-on voltage V_T

$$V_T = -2\psi_B + V_{fb} - \frac{\sqrt{2\varepsilon_s q N_D(2\psi_B)}}{C_i} \qquad (1.7)$$

In this region, the transconductance

$$g_m = \frac{\partial I_D}{\partial V_G} = \frac{Z}{L}\mu_p' C_i V_D \qquad (1.8)$$

& the drain conductance

$$g_D = \frac{\partial I_D}{\partial V_D} = \frac{Z}{L}\mu_p' C_i (V_G - V_T) \qquad (1.9)$$

As the drain voltage is increased, the gate voltage may not be sufficient to induce an inversion layer near the drain, so that a depletion region exists between the channel

and the drain. Further increase of V_D is dropped across the depletion region and the voltage across the channel remains equal to a saturation drain voltage V_{DS}. The value of V_{DS} can be found from Eq. 1.3 by putting $Q_p(y) = 0$ at the drain.

Some deviations from the above ideal theory exist for practical devices.

1. Effective mobility of carriers in the channel

The assumption that the mobility of carriers is constant in the channel is not valid at very low and very high gate voltages. At low gate voltages, when the carrier concentration in the channel is low and there are many traps at the $Si-SiO_2$ interface, the effective carrier mobility can be greatly reduced. [5] This is because some carriers in the channel are trapped, and the mobile carrier concentration is less than that if there are no traps present. This can be accounted by a lowered effective mobility μ'_p. For a P-channel

$$\mu'_p = \mu_p \left(\frac{Q_p - Q_T}{Q_p} \right) \qquad (1.10)$$

where Q_T = concentration of holes in the trapped states

Q_p = concentration of holes in the channel if no traps are present

μ_p = bulk hole mobility

Equation 1.10 can be obtained since the mobility of trapped charge is zero.

At high gate voltage where the concentration of holes in the channel is much greater than that trapped in the surface states, $\frac{Q_p - Q_T}{Q_p} \rightarrow 1$, and μ_p' approaches μ_p .

At very high gate voltage, the field in the oxide is so high that carriers are continuously attracted to the interface at $Si-SiO_2$ and scattered, since the interface must be uneven and imperfect. This scattering effect thus reduces the carrier mobility just like lattice and impurity scattering. This effect has been studied by Schrieffer [6], who obtained

$$\frac{\mu_p'}{\mu_p} = 1 - \exp[\alpha^2]\, \operatorname{erfc}[\alpha] \qquad (1.11)$$

$$\text{where } \alpha = \frac{1}{E_s \mu_p} \sqrt{\frac{2kT}{m^*}}$$

where m^* is the effective mass of carriers

E_s is the surface electric field

2. Saturation drain resistance

In actual MOST, the drain current is not constant after the channel is pinched off, but shows slight increase as V_D is increased. Two effects are usually attributed to the saturation drain conductance g_{DS} : the modulation of the channel length by the drain voltage, and the drain-to-channel feedback effect. [7,8] These are illustrated in Fig. 1.2 .

After saturation, a depletion region of length ΔL

exists between the channel and the drain. The value of ΔL is affected by the voltage drop $(V_D - V_{DS})$ across the depletion region as in a reverse biased junction. The value of ΔL is given by

$$\Delta L = \left[\frac{2\varepsilon_s |V_D - V_{DS}|}{qN_D}\right]^{\frac{1}{2}} \qquad (1.12)$$

The saturation drain conductance g_{DS} can be shown to be

$$L\left(\frac{\varepsilon_s}{2qN_D}\right)^{\frac{1}{2}} I_{DS}(\text{ideal}) \Big/ \left\{L - \left[\frac{2\varepsilon_s |V_D - V_{DS}|}{qN_D}\right]^{\frac{1}{2}}\right\}^2 |V_D - V_{DS}|^{\frac{1}{2}} \qquad (1.13)$$

Eq. 1.13 predicts that g_{DS} is proportional to I_{DS}. The channel modulation effect is especially important in short channel devices.

The drain-to-channel feedback effect arises because some electric lines of force from the bound charge in the drain contact region tend to terminate on the channel and hence induce additional carrier concentration in the channel near the drain. This effect is more important in lightly doped bulk devices because the flux from the drain charge cannot terminate completely on the ionised atoms in the depletion region. The saturation drain conductance due to feedback has been calculated [4] for a lightly doped bulk as

$$g_{DS} = \mu_p' \frac{Z}{L^2} \varepsilon_s (V_G - V_T) \qquad (1.14)$$

1.2 Effect of illumination on a surface space charge region due to interband transition of carriers

The effect of illuminaiom on a surface space charge

in semiconductors causing transition of carriers between the conduction and and valence band has been studied by the measurement of surface photovoltage. The surface photovoltage in Ge under such illumination was first studied by Garett and Brattain [9]. Johnson [10] investigated the surface photovoltage under high level of illumination and the effect of surface states. Other work have then been done in studying the surface photovoltage in other semiconductors and MOS capacitors.[11-14] The surface depletion barrier, surface state properties and bulk minority carrier lifetime have all been studied using the surface photovoltage method.

Under optical generation of carriers in the bulk, there is in general re-distribution of carriers in the surface space charge region. The quasi-Fermi levels E_{FP} E_{FN} under illumination are assumed flat within the surface space charge region if the diffusion current can be neglected. Poisson Equation can be applied to solve for the space charge distribution. [10]

Space charge per unit area $Q_s^* = \mp 2n_i q L_D F_s^*$

where $F_s^* = [\lambda(e^{-u_s^*} + u_s^* - 1) + \lambda^{-1}(e^{u_s^*} - u_s^* - 1) + \lambda(e^{u_s^*} + e^{-u_s^*} - 2)\Delta_p]^{\frac{1}{2}}$ (1.15)

$$p_o^* = p_o + \Delta p_o$$
$$n_o^* = n_o + \Delta n_o$$
$$\Delta p = \Delta n$$
$$\Delta_p = \frac{\Delta p_o}{p_o}$$
$$\Delta_n = \frac{\Delta n_o}{n_o}$$
$$\lambda = \left(\frac{p_o}{n_o}\right)^{\frac{1}{2}}$$

Q_s in darkness can be found from Eq. 1.15 by putting $u_s^* = u_s$ and $\bar{\Delta}_p = 0$. Eq. 1.15 indicates that Q_s^* is greater than Q_s at the same surface potential $u_s^* = u_s$. If the time constant of the external circuit is large enough, charge neutrality of the system requires that the sum of the semiconductor space charge and surface state charge remains constant under illumination.

$$Q_s + Q_{ss} = Q_s^* + Q_{ss}^* \qquad (1.16)$$

In general, $|u_s^*| < |u_s|$, and there results in a surface photovoltage.

In this project, the responses of the MOST to light causing interband transition of carriers in the semiconductor under the gate were studied. Compared with the MOS-capacitor, we are investigating the effect of illumination on the surface space charge under non-equilibrium conditions, i.e. with a drain current flowing. An accurate analysis of the problem seems very complex due to the presence of the optical generation term in the continuity equations for the system. Some recent work on the numerical solution of the MOST characteristics may provide some reference to the problem.[15,16] However, we shall try to observe the MOST photocurrent experimentally, and then induce from the experimental results some properties of the MOST under optical injection of carriers. The results will be discussed in Chapter 3.

1.3 Direct excitation of surface state carriers by optical absorption

Surface photovoltage measurements have been effectively used in the study of semiconductor surfaces using photons of energy greater than the bandgap. Very intense light was used to flatten the energy band in the semiconductor and thus the surface potential barrier was measured from the saturation surface photovoltage [10,13], or the surface state density could be derived from the slope of the curve of surface photovoltage as function of the logarithm of light intensity. [11,14]

Recently, a new technique called the surface photovoltage spectroscopy has been successfully applied to some high bandgap semiconductors with a surface barrier such as CdS and Ga As. [17-20] The method uses monochromatic light of energy less than the bandgap. The principle is that if the photon energy is of the right magnitude, electrons or holes at the surface states may be excited to the conduction or valence band. This results in a population or depopulation of electrons at surface states. For charge neutrality, the surface space charge in the semiconductor is altered and results in a change of the surface potential.

An extensive and comprehensive work on surface photovoltage spectroscopy in CdS was carried out by Balestra et al. [17-20] The distribution of the surface states within the energy bandgap was determined from the spectrum of the surface photovoltage over a range of photon energies below the bandgap.

Fig. 1.4 shows a typical spectrum of the surface photovoltage in CdS crystals[20]. The derivative of the surface photovoltage with respect to photon energy shows definite maximums which are attributed to the direct excitation of electrons from a surface state to the conduction band . Thus surface states at energies 0.8 eV, 1.1 eV below the conduction band were found to be present. The assumption is of course that direct excitation of electrons only occurs when the photon energy exceeds the energy difference between the conduction band and the surface state.

The surface potential has been found both to decrease and increase under illumination depending on the light wavelength.[18] The decrease in surface potential was explained by an excitation of electrons to the conduction band and decreasing the surface depletion width (in a N-type bulk). The increase of surface potential, called the inversion effect, was due to the excitation of holes from the surface state to the valence band. These holes recombine

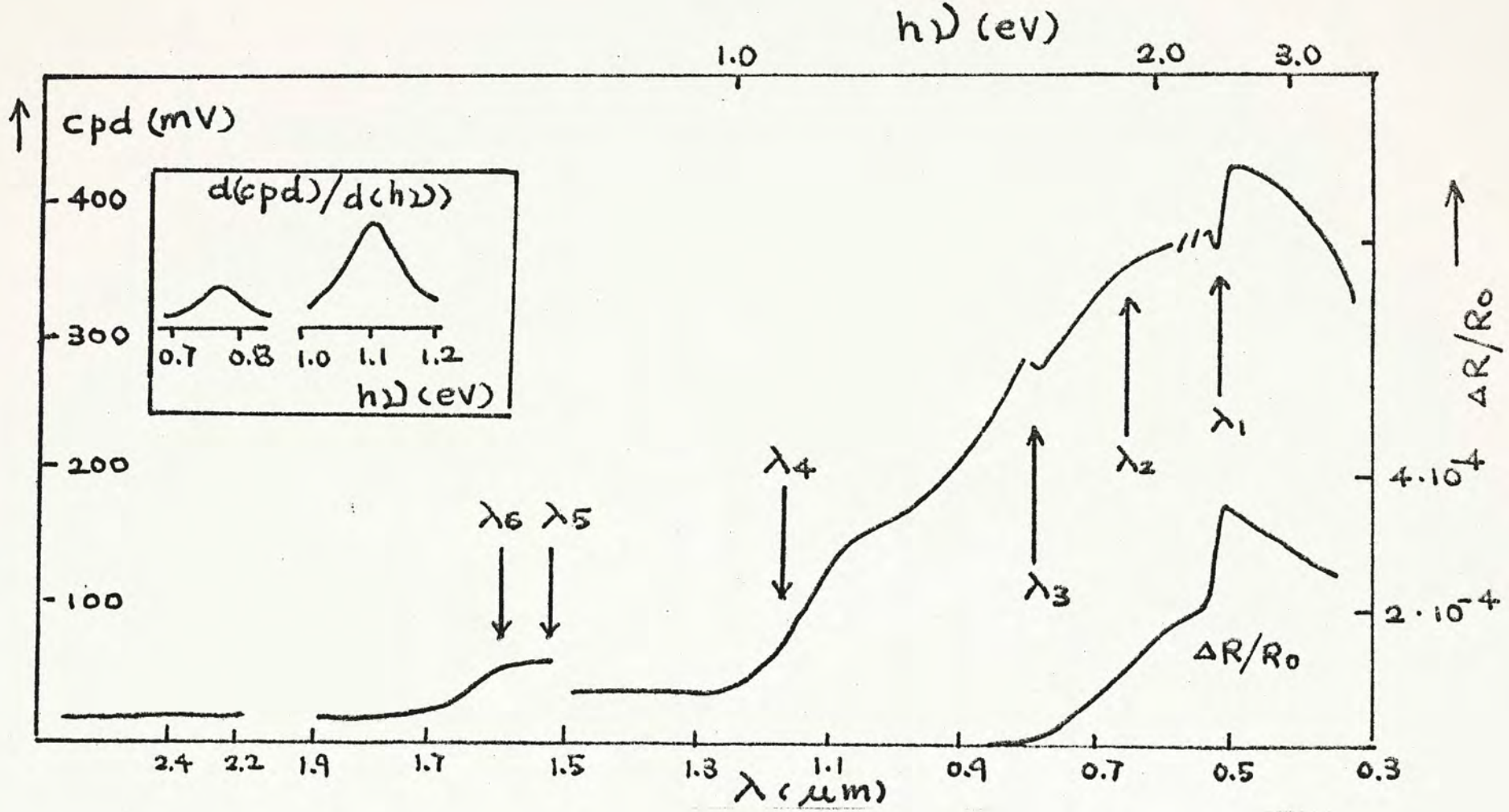

Fig.1.4 Surface photovoltage spectrum and photoconductivity of the prismatic surfaces of CdS in room temperature Ref 20

quenching of surface photovoltage occurs at λ_1 λ_3

with electrons in the conduction band and increase the surface depletion width. (Fig. 1.5)

Dips in the surface photovoltage spectrum,[20] corresponding to sudden increase of the surface potential, were also observed (Fig 1.4) Such quenching was explained by the excitation of holes from the surface state to the valence band, but they occurred at photon energies greater than half the bandgap.

An important phenomenon observed by Balestra et al was that the time constant associated with the excitation of carriers from a set of surface states was significantly different from those of other surface states, and that the photovoltage measured could be attributed to a set of surface states only.[19] From the transients of the photovoltage, it was shown that the thermal capture cross section, optical capture cross section for photons, the occupation probability by electrons, and the density of surface states could all be deduced. From the spectrum and the transient response of the surface photovoltage, detail information on the surface states leading to electronic characterization of the CdS surface has been obtained.[20]

In this work, the semi-transparent gate MOST was used as a means of observing the effects of direct optical absorption by Si-SiO_s interface states. The photocurrent in the MOST under monochromatic sub-bandgap illumination was measured. The results will be discussed in Chapter 4.

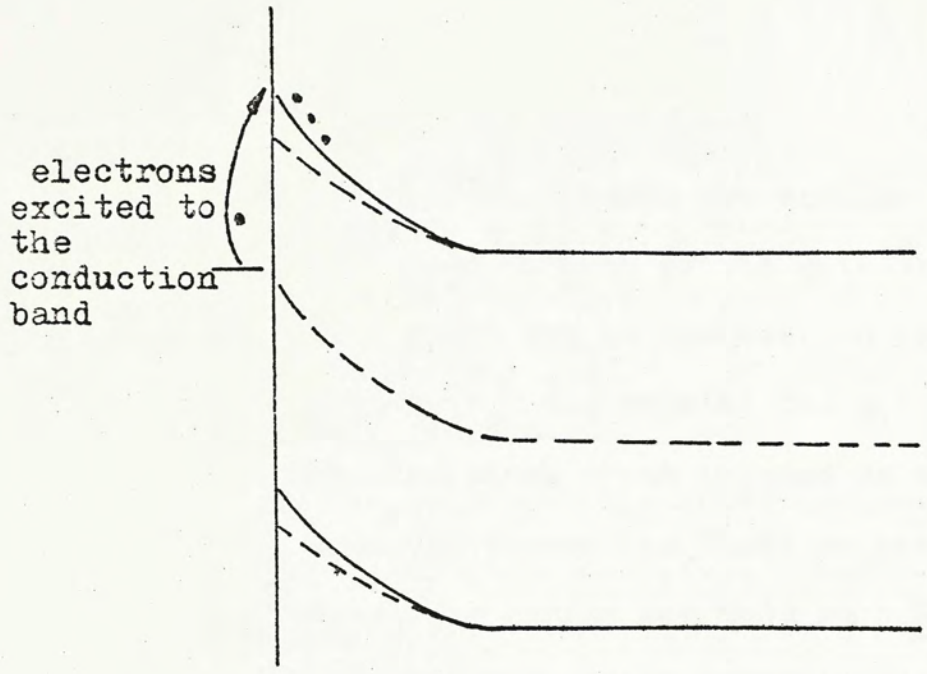

(a) ψ_s decreases

• electrons

o holes

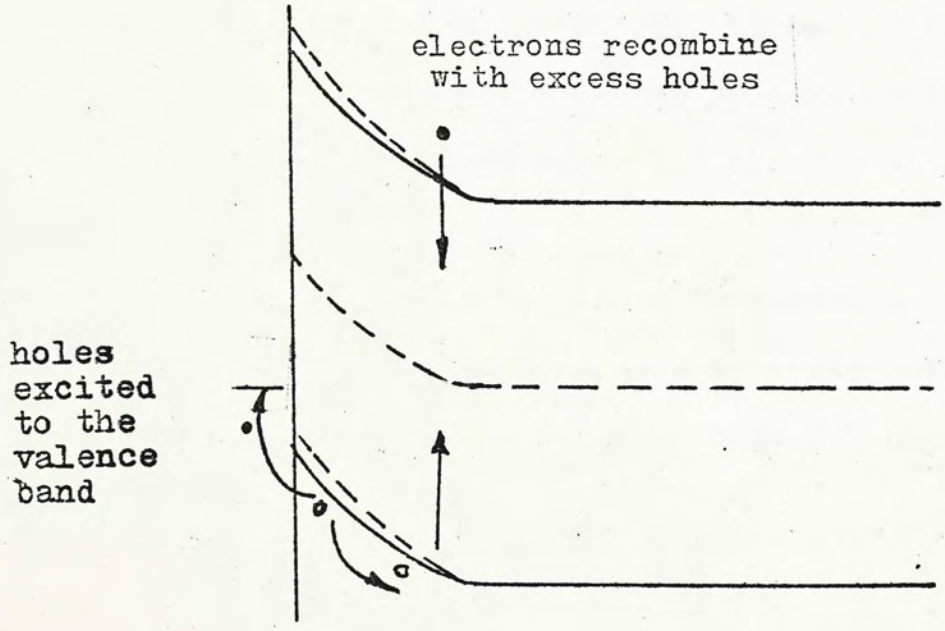

(b) ψ_s increases

Fig.1.5

II. Fabrication of samples

2,1 Structure of the MOST samples fabricated

The samples used in the experiments are similar to the conventional MOST, except that most part of the gate electrode is semi-transparent so that light can be transmitted into the semiconductor under the gate. The edge of the gate electrode is normal thick aluminium, which is used as the probing contact and a means of preventing light to reach the source and drain junctions. The sample was made much larger than the commercial transistors for optics convenience. The cross section and the plan of electrode patterns are as shown in Figs. 2.6, 2.1d respectively.

2.2 Fabrication procedures

The samples were fabricated on n-type (111) Si wafers of resistivity in the range 1-3 ohm-Cm. Cleaniness of the wafer was maintained between steps in the process by rinsing with trichloroethylene, deionised water and blowing with dry, filtered nitrogen.

The masks used in the fabrication were produced by standard photolithographic techniques from artworks marked on Stabilene cutting strips by a Scriber. Fig. 2.1 show the dimensions of the set of masks used.

The fabrication procedures are described below:

1. A layer of SiO_2 of about 6000 Å was thermally grown on the wafer by steam oxidation at a temperature of 1100°C. Oxygen carried by steam was passed at a rate of 1 litre/min. for 40 minutes. This oxide layer served as a passivation barrier for selected diffusion.
2. A few drops of KMER (Kodak Metal Etching Resist) were applied on the wafer, which was then spinned at a speed of 3000 r.p.m. to obtain an even coating of KMER on the wafer. The coating was dried by evaporation at 80°C for 35 minutes.
3. The wafer was carefully aligned with Mask 1 for obtaining the diffusion pattern on a Mask Aligner, and was then exposed by a collimated beam of ultraviolet light. The KMER film was then developed, and finally hardened by heating at 150°C for 30 minutes.
4. The oxide beneath the unexposed KMER was removed by a 4:1 buffer solution of NH_4-HF in order to achieve a constant etching rate. The KMER film was then removed by heating in chromic acid.
5. The wafer with patterned openings in the oxide was ready for the source and drain diffusions. In this laboratory, solid state diffusion by the spin-on technique was used. Borosilicafilm was used as the liquid dopant source.

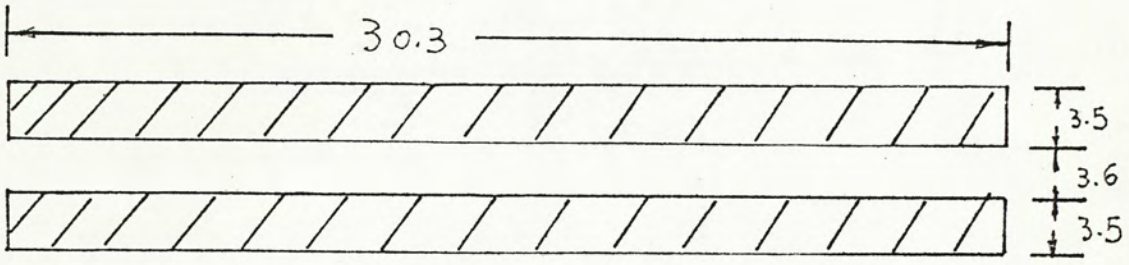

Fig.2.1 (a)Mask 1

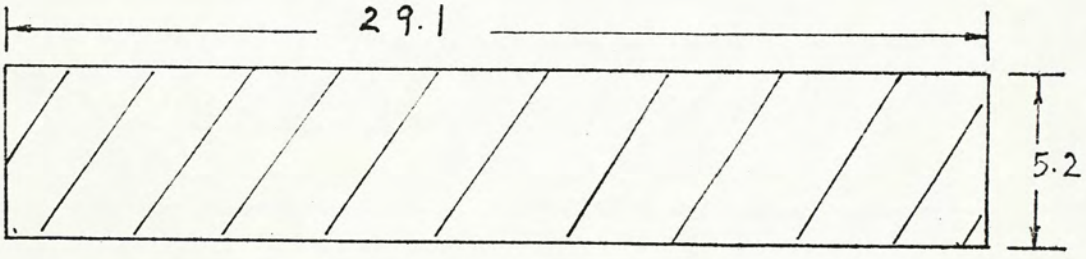

Fig.2.1(b) Mask 2

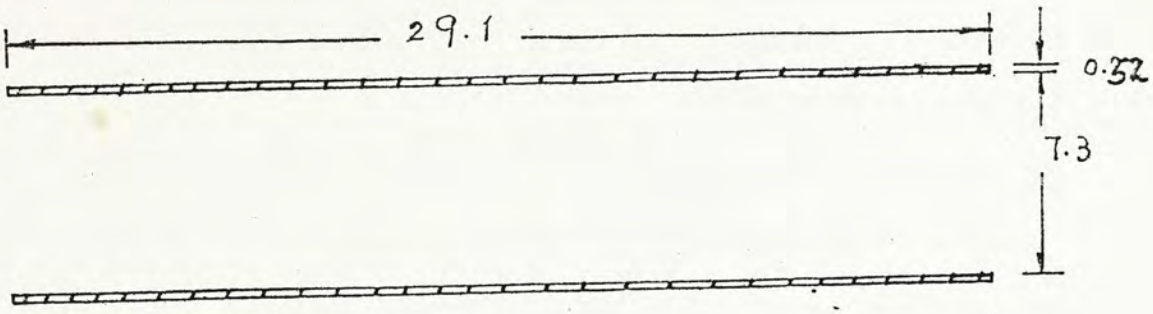

Fig.2.1 (c) Mask 3

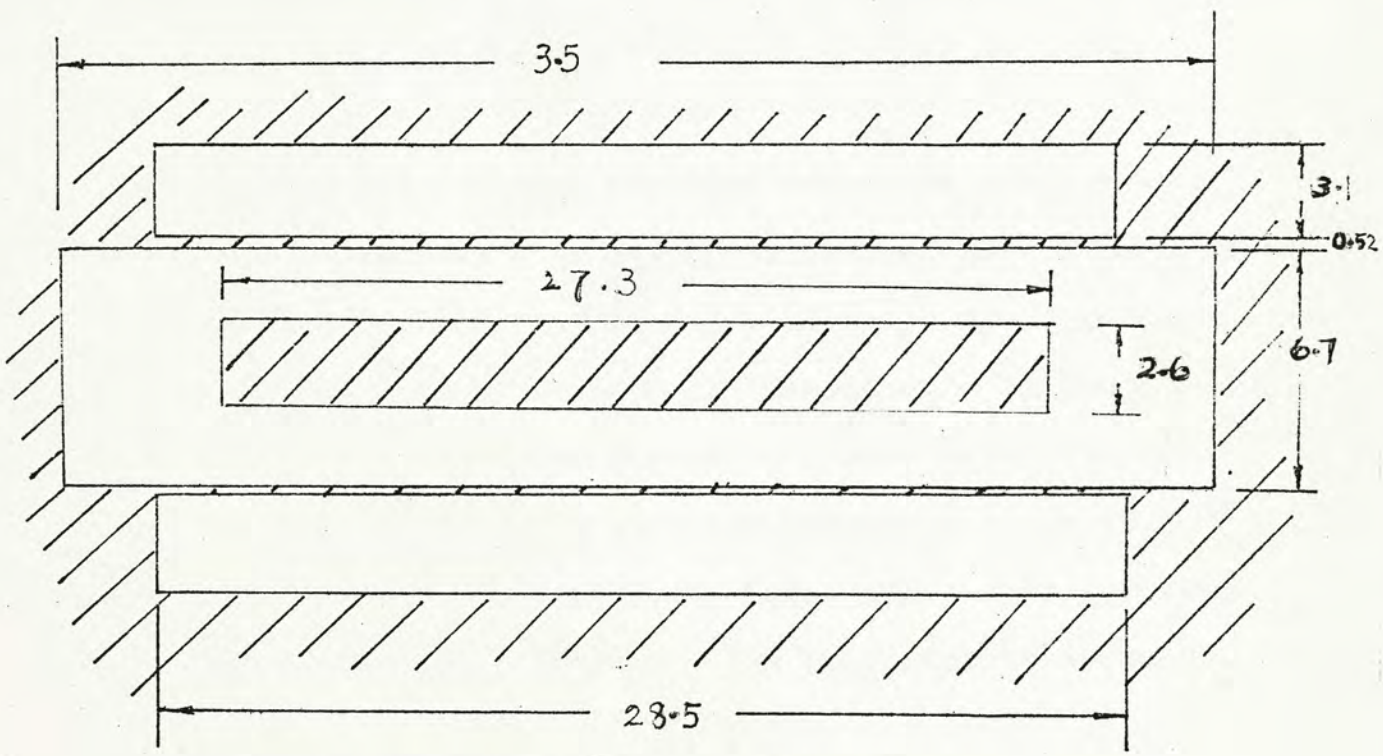

Fig. 2.1 (d) Mask 4

Mask 5 is the negative of mask 2.

Fig. 2.1 Masks for the fabrication of samples.. Shaded portions are opaque. Dimensions in $^{1}/_{c}$mm.

Sufficient material was applied so that the wafer was completely covered with the solution. After 20 seconds of wetting, the wafer was spinned for 20 seconds at 4000 r.p.m. Residual solvent was removed by heating at 70°C for 15 minutes and the film was hardened at 250°C for at least 30 minutes. Diffusion then took place at a temperature of 1000°C for 30 minutes in an open furnance with an ambient of nitrogen flowing at the rate of 1 lit./min. The diffused p regions would have a surface concentration of 10^{19} cm^{-3} and a sheet resistivity of 60 -80 ohms/sq.cm. The residual film after diffusion was removed by rinsing in 10:1 H_2O : HF solution. (Fig. 2.2)

6. The photoresist and etch sequence described above was repeated using Mask 2 to obtain an opening in the oxide at the gate region. A thin layer of oxide was then grown over the wafer in a double-wall furnace at a temperature of 1100°C . Dry oxygen was passed at a rate of 1 lit./min for 1 hour, resulting in an oxide thickness of about 1400 Å. Nitrogen was passed through the outer wall of the furnace to prevent ion contamination. The oxide was subsequently subjected to annealing under nitrogen atmosphere at about 500°C for 30 minutes. (Fig. 2.3)
7. Mask 3 was used to make openings in the oxide at the source and drain for ohmic contact. (Fig. 2.4) A thick layer of aluminium was then evaporated on the wafer under a

Fig. 2.2 to 2.6 refer to the structures of the sample during fabrication steps

Fig. 2.2

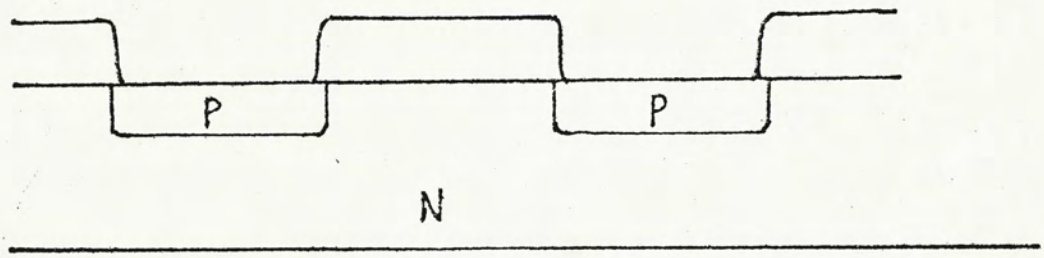

Fig. 2.3

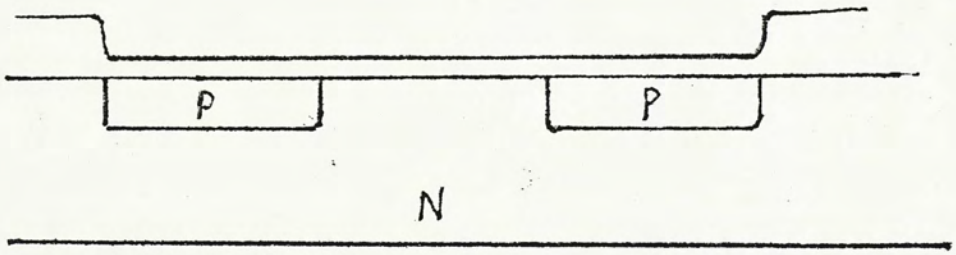

Fig. 2.4

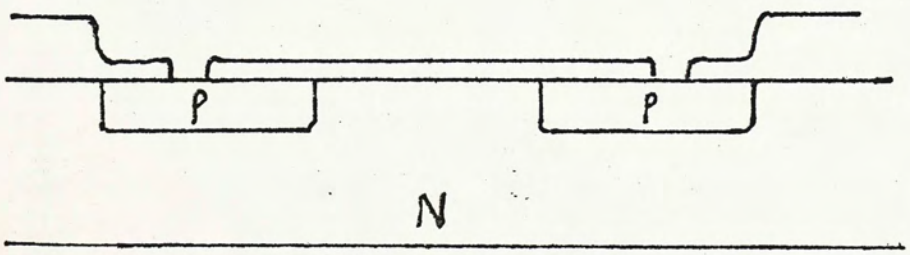

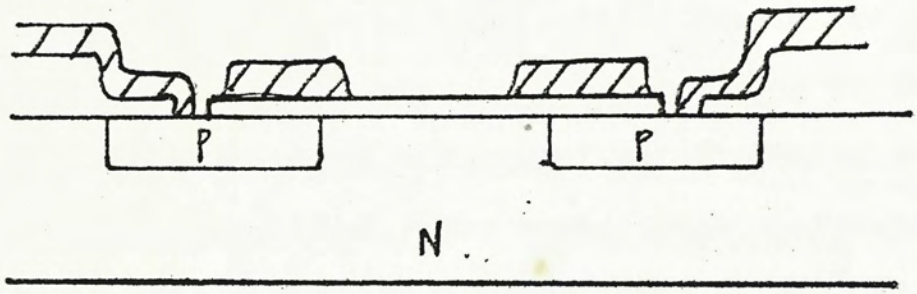

Fig. 2.5

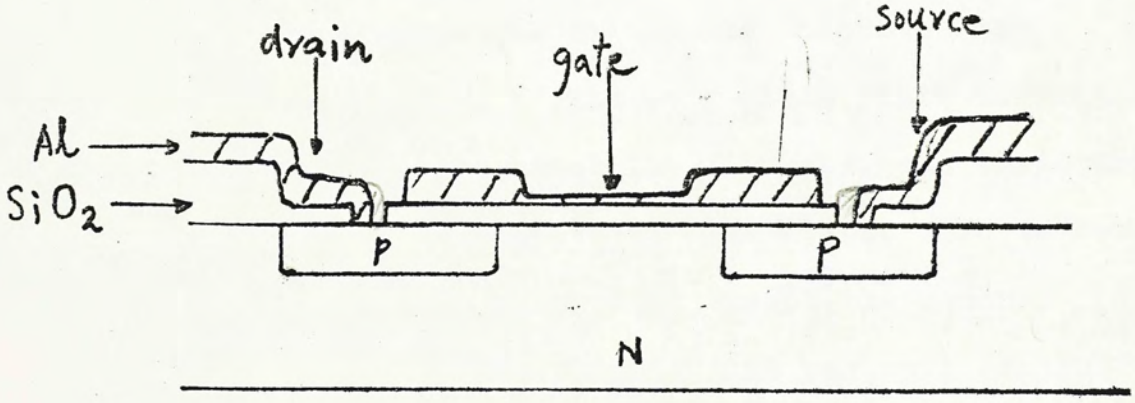

Fig. 2.6

pressure of 10^{-5} torr. in a vacuum evaporation unit.

8. Mask 4 was used to remove the aluminium layer between the source, gate and drain electrodes, and over the central gate region. The photoresist process was the same as that described before. A 4:1:10 mixture solution of H_3PO_4 : HNO_3 : H_2O was used to etch the aluminium, and Chemical Strip Reagent was used instead of chromic acid to remove the developed KMER film. The Chemical Strip remaining on the wafer was dissolved in equal mixture of trichloroethylene, acetone and isopropylalcohol. The contacts at the source and drain were then alloyed at a temperature of 500° C for 20 minutes in nitrogen ambient. (Fig. 2.5)
9. A thin film of semi-transparent aluminium was then evaporated on the wafer. The aluminium thickness was controlled by the opening time of the shutter and current setting of the filament in the evaporation unit. The thickness was monitored by evaporating a film on a glass plate under the same conditions to ensure that the film was semi-transparent.
10. Mask 5, which was the negative of Mask 2, was used to remove the thin aluminium film evaporated except the central region over the gate. The etching time was well controlled so that the thick aluminium layer for ohmic contacts at the electrodes was not affected. The final structure of the sample is shown in Fig. 2. 6 .

III. Response of the MOST to photons of energy greater than the Si bandgap

3.1 Introduction

In this chapter, the photo-response of the MOST to illumination causing transition of carriers between the energy bands in the Si bulk under the gate will be described. The photocurrent under such illumination has been measured as functions of the drain and gate voltages at different light intensity. The mechanisms responsible for the photocurrent in the MOST are discussed from the experimental results.

3.2 Experimental Method

The experimental set up was as shown in Fig. 3.1 . Details of the MOST sample used has been described in chapter 2. Contacts to the electrodes of the sample were made by means of probes which could be adjusted in the x,y,z directions. Light from a commercial Tungsten Halogen projector lamp was chopped at a frequency of about 70 Hz and then focussed on the sample. A highly regulated power supply was used for the lamp to ensure that the light intensity remained constant during the measurement. The increase of the drain current under illumination resulted in a voltage signal across the 100 ohm resistor in the source circuit, which was amplified by the Low Noise Amplifier. The output from the Low Noise Amplifier was fed to

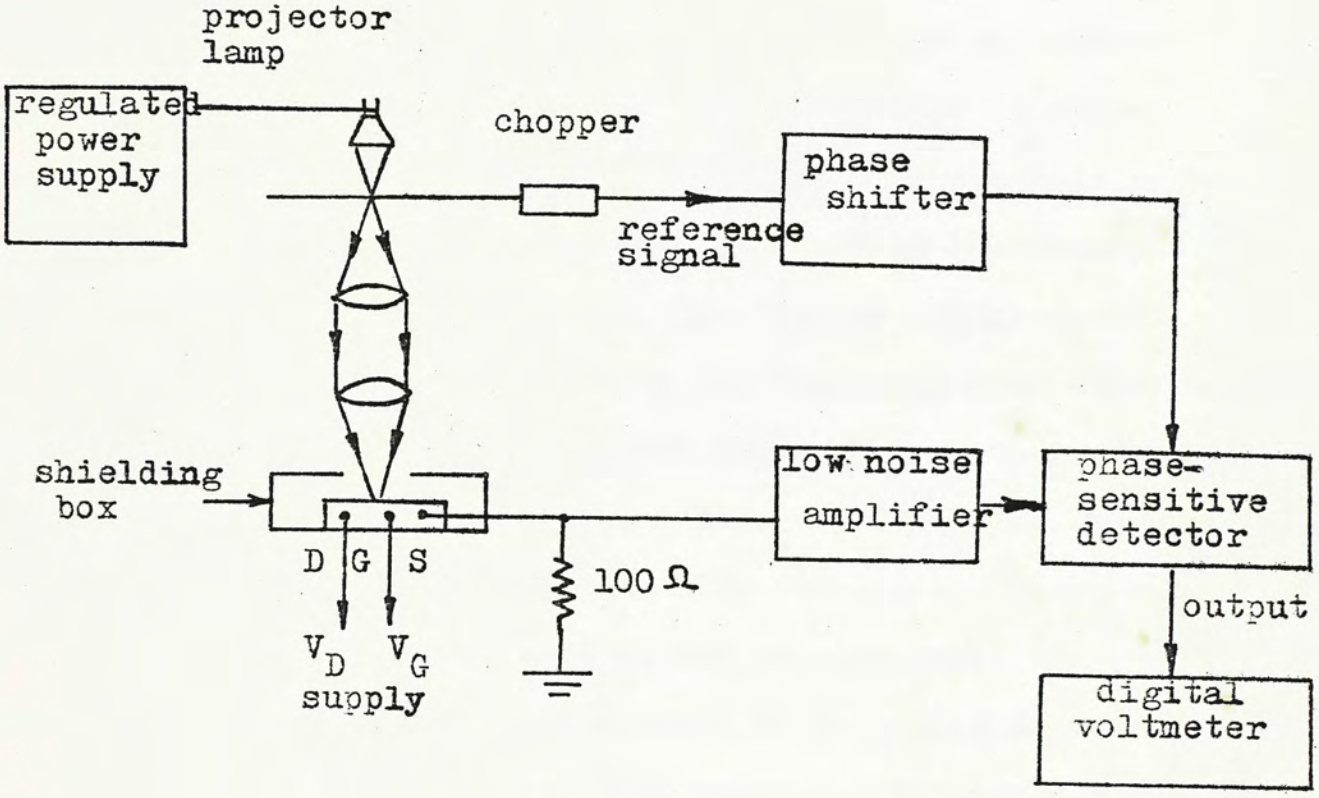

Fig.3.1 Experimental set up for measuring the photocurrent

the Phase Sensitive Detector. A reference signal was provided by a photo-transistor receiving the light from a small light bulb passing through the chopper. The phase shift of the reference signal was adjusted until the detector output was maximum, indicating that the input signal and the reference signal were in phase. The phase shift detector system provided an accurate measurement of the photo-signal even in the presence of noise.

The possibility of emission of charges from the gate to the semiconductor was excluded because no gate current was observed under illumination. It was also checked that no signal across the source resistor was detected when the drain was open circuited. Thus the photocurrent measured must be due to the photogenerated carriers in the Si bulk between the source and the drain, and not related to any optical effects at the junctions. Since only moderate light intensity was used in the measurements, the heating effect of the sample was assumed to be negligible.

The relative flux densities of photons with energy greater than the bandgap were measured at different light bulb voltages from the surface photovoltage of an MOS capacitor biased to strong inversion. Details of the method are described in the Appendix.

3.3 Experimental results

For our p-channel sample, the drain voltage, gate voltage, and turn-on voltage are all negative (with respect to the source). Fig. 3.2 shows the characteristics of a typical sample with

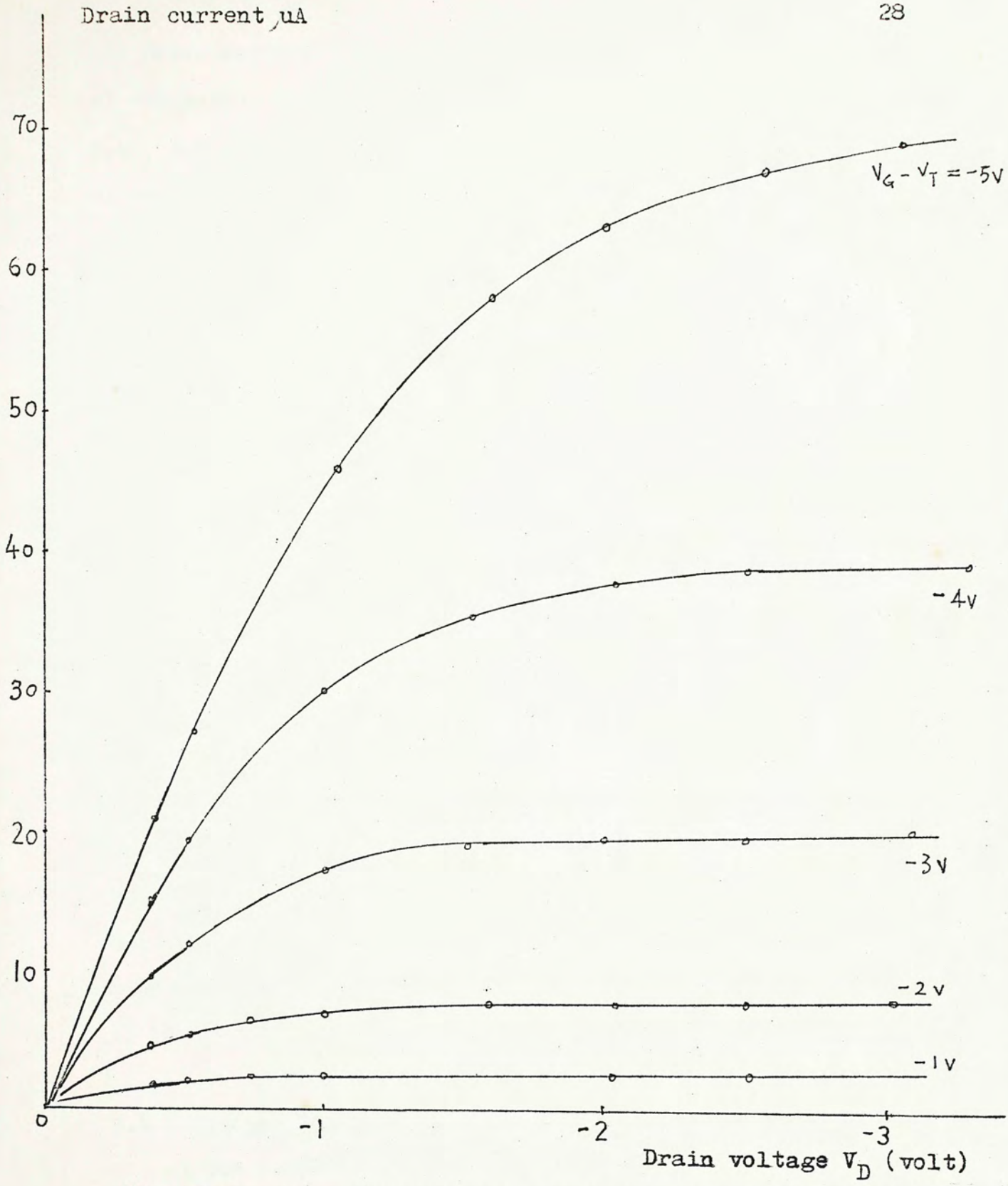

Fig. 3.2 Characteristics of a typical p-channel MOST fabricated

the drain current I_D plotted against the drain voltage V_D at different gate voltages V_G . Figs 3.3a, 3.3b, 3.3c, 3.4 , 3.5 , 3.6 , 3.7 show the corresponding photo-response of the sample at different light intensity F_1, F_2, F_3 ($F_1 < F_2 < F_3$).

The dependence of the photocurrent I_p of the MOST on the gate voltage at a fixed drain voltage of-0.5 volt was measured under various light intensity (by varying the light bulb voltage). The results are shown in Fig, 3.3 . It was found that the photocurrent at all light intensity was constant for gate voltages below a value about $|V_T| - 1.5$ volts where V_T is the turn-on voltage, but started to rise at higher gate voltages. At sufficiently high gate voltages, the rate of increase of the photocurrent was reduced.

Figs. 3.4, 3.5, 3.6 show the dependence of the photocurrent on the drain voltage at various gate voltages. It was observed that at gate voltages corresponding to the flat portion of the photocurrent in Fig. 3.3, the photocurrent was also independent of the drain voltage. But at higher gate voltages, the photocurrent first increased with the drain voltage, but then decreased as the drain voltage was furthur increased. Similar phenomena were observed at different light intensity, except that the width of the peak region seemed to increase under stronger illumination.

3.4 Discussion of the results

The experimental results obtained in the last section

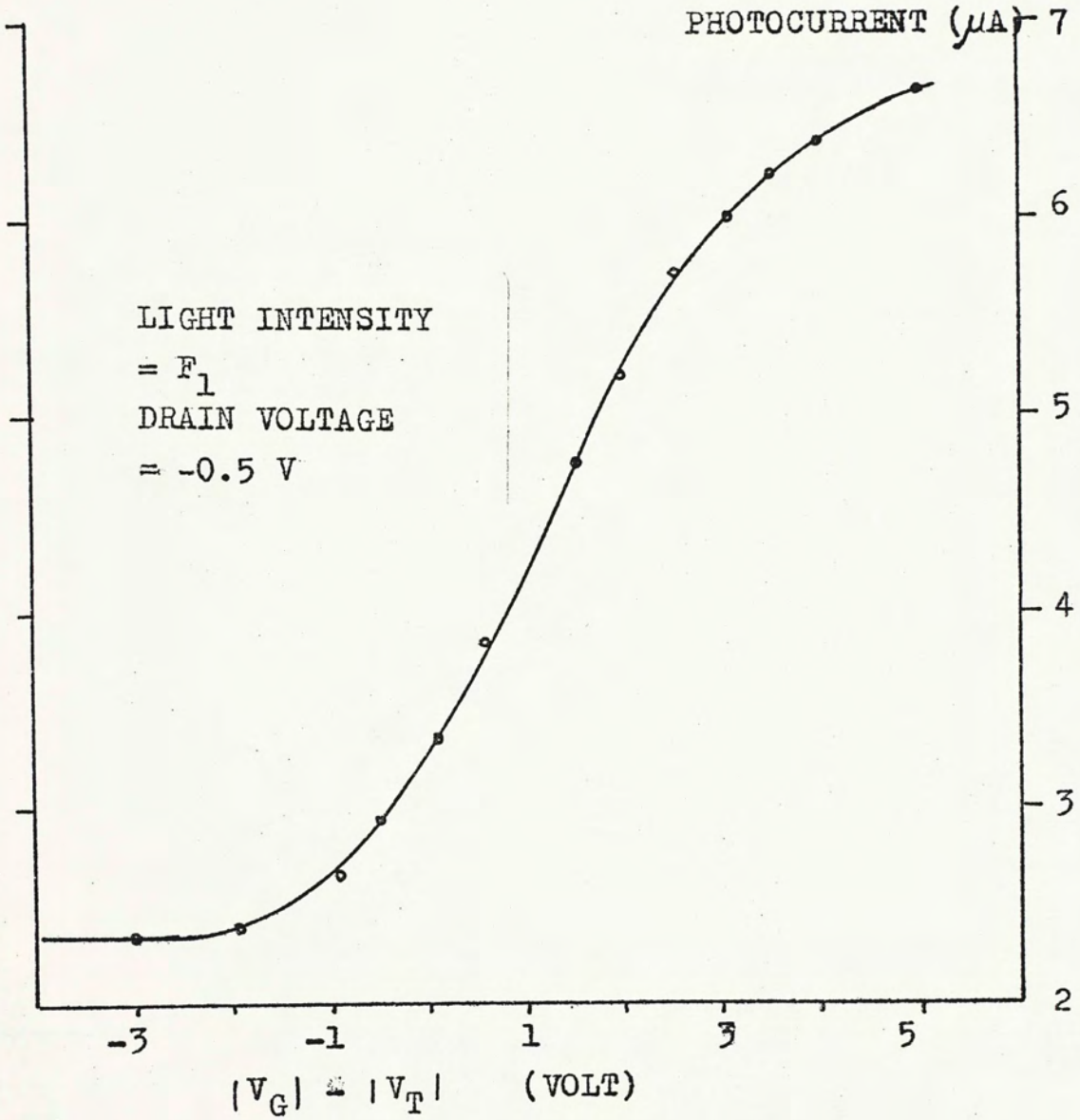

FIG 3.3 (a) Variation of photocurrent with gate voltage.

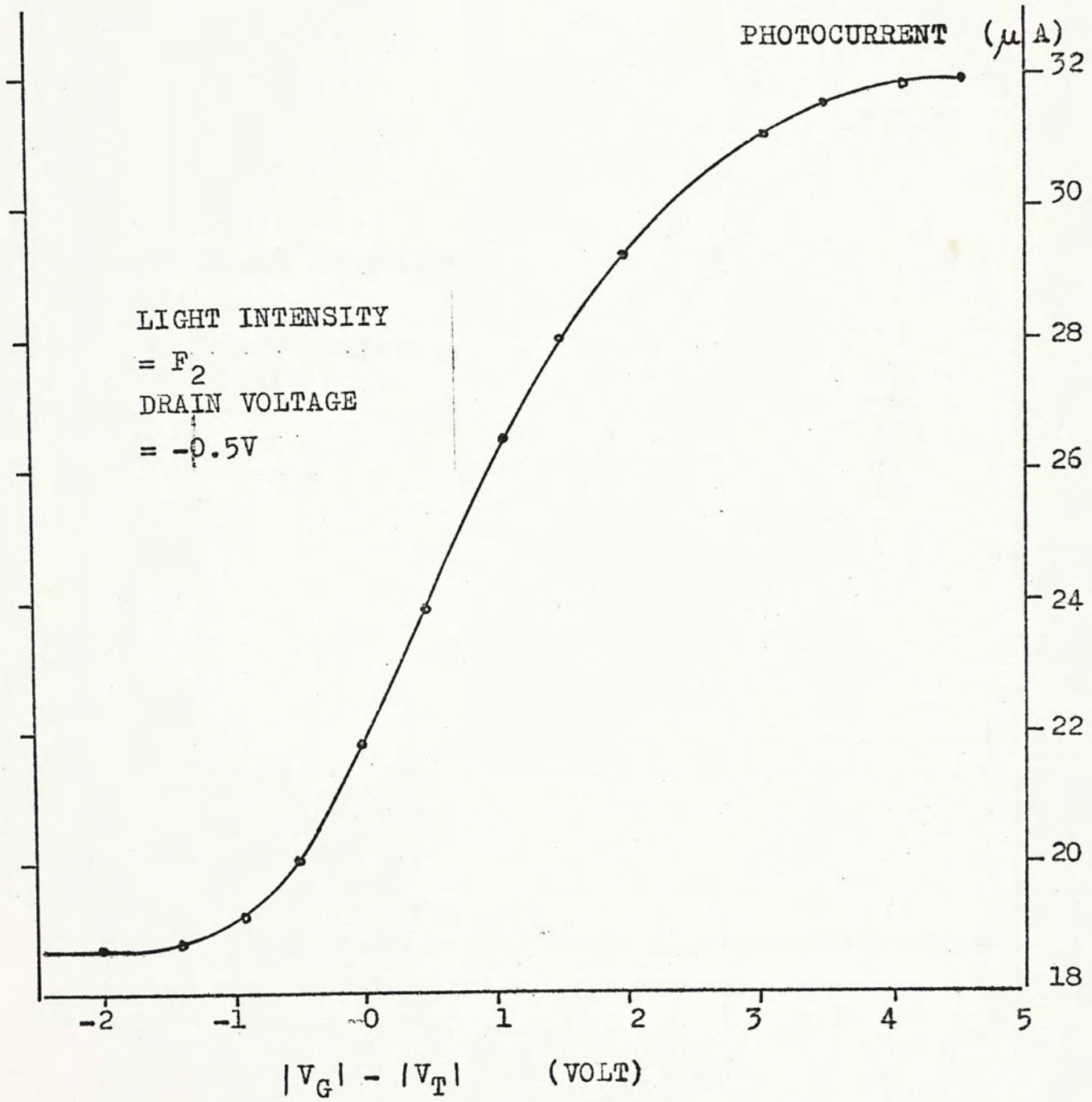

Fig 3.3 (b) Variation of photocurrent with gate voltage.

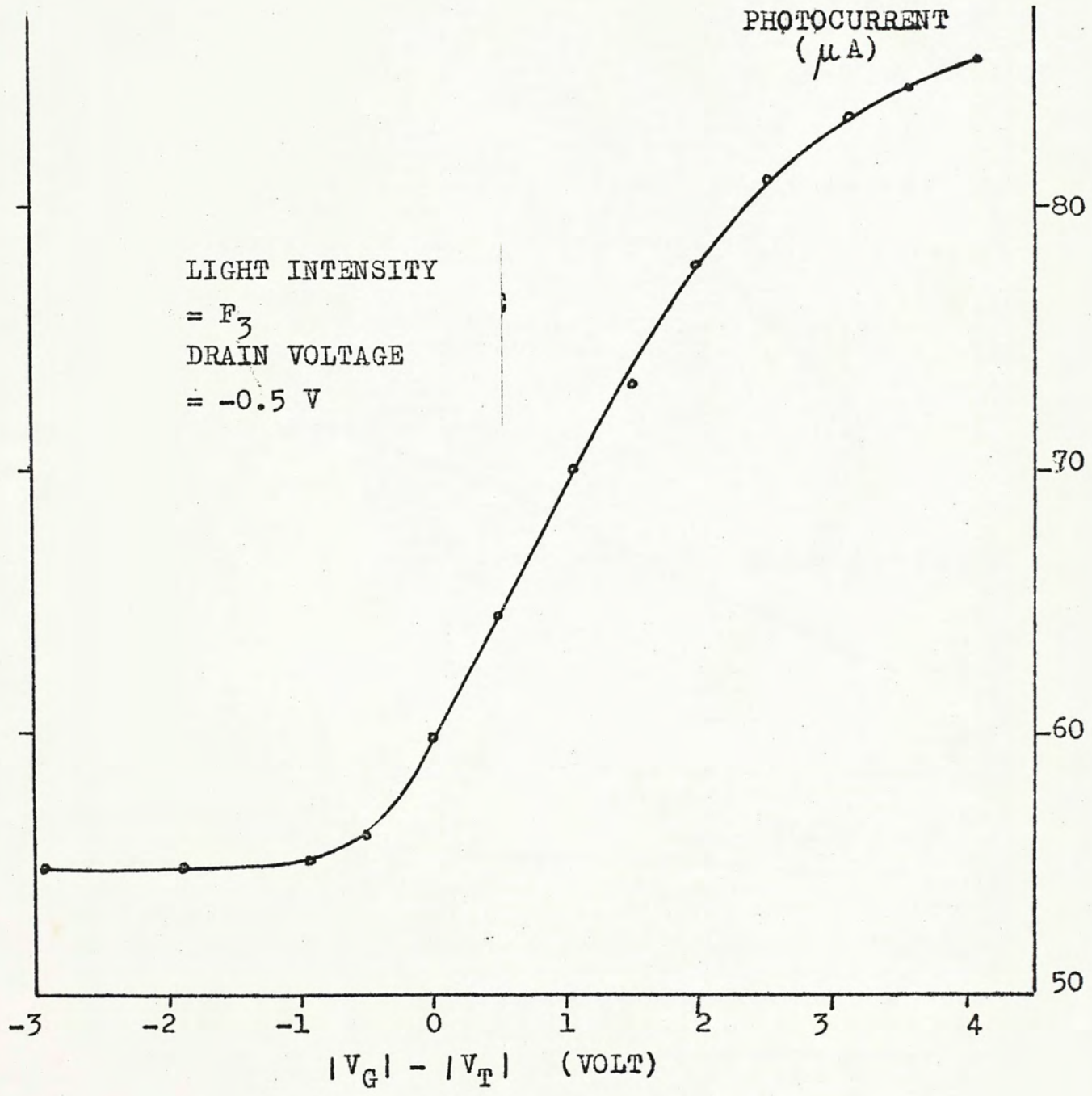

FIG 3.3 (c) Variation of photocurrent with gate voltage

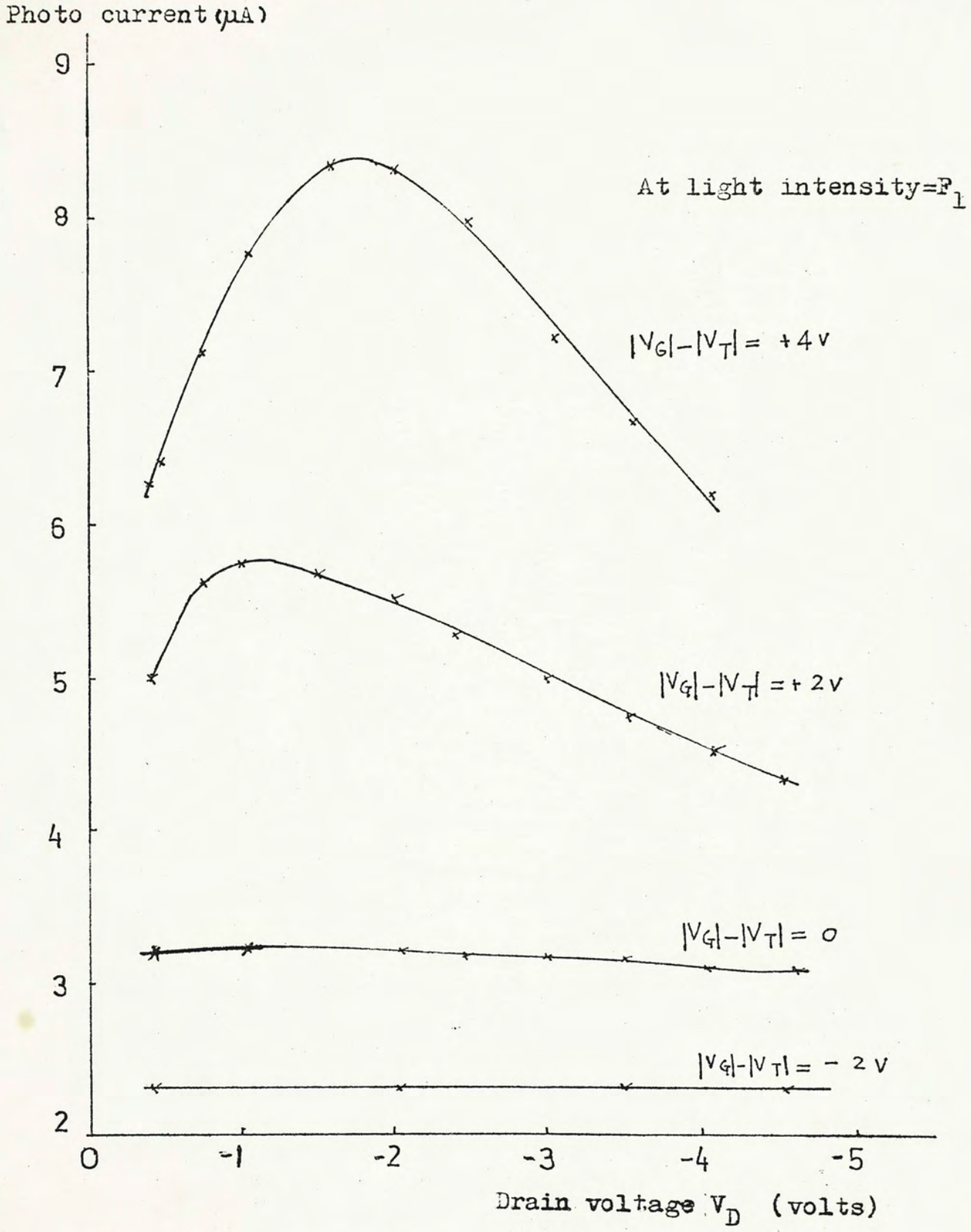

Fig. 3.4 Variation of photocurrent with drain voltage.

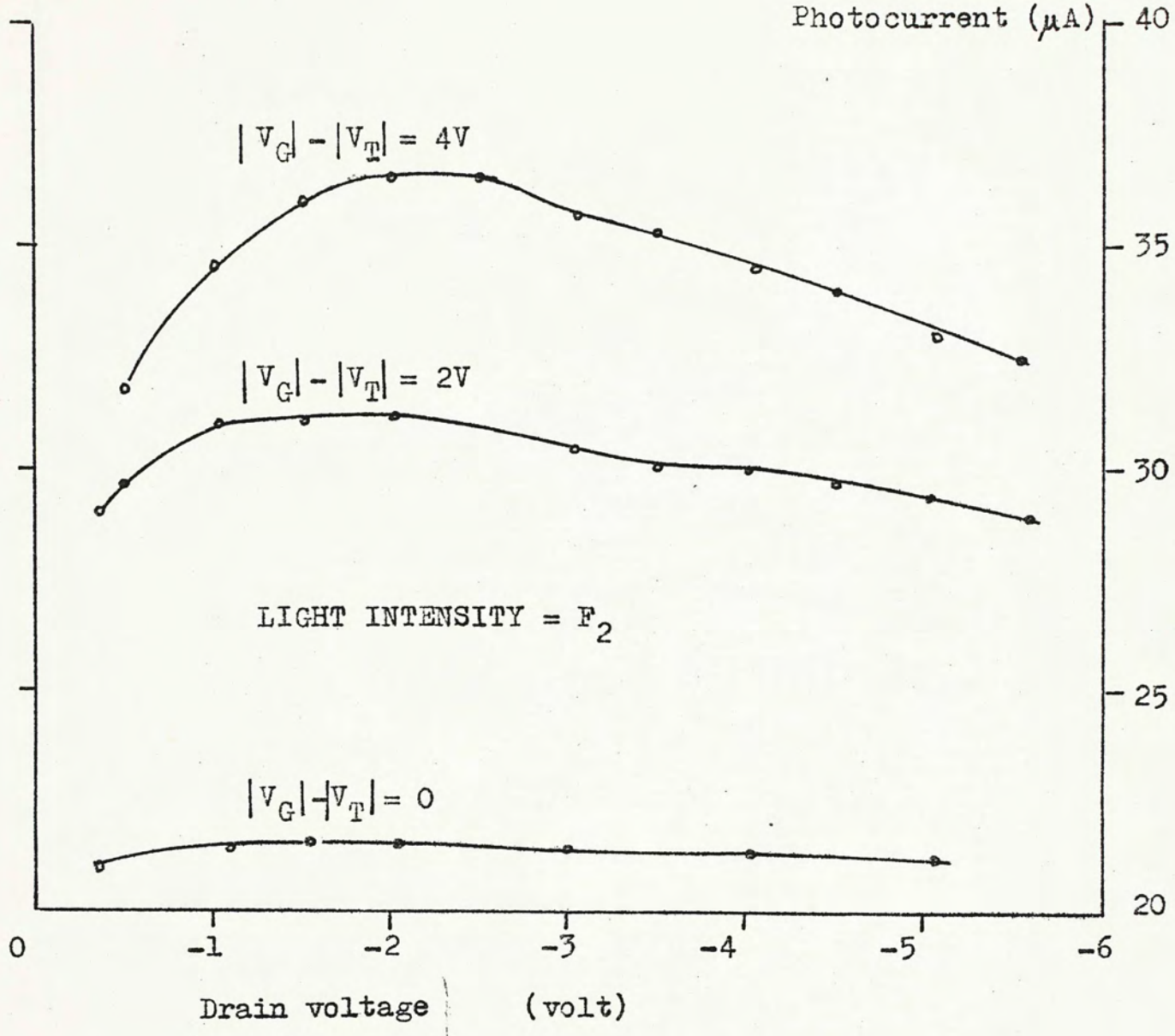

Fig 3.5 Variation of photocurrent with drain voltage.

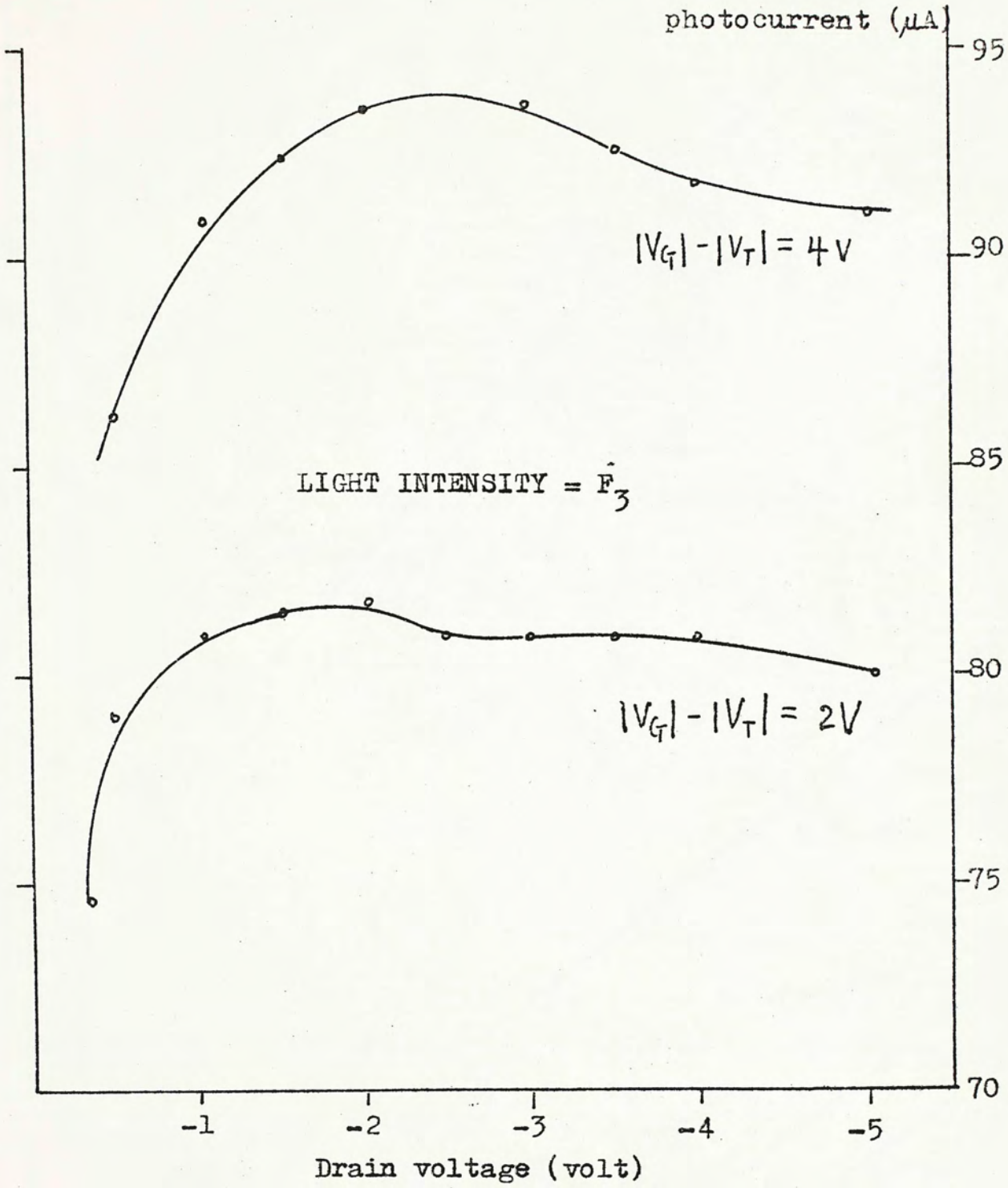

Fig 3.6 Variation of photocurrent with drain voltage.

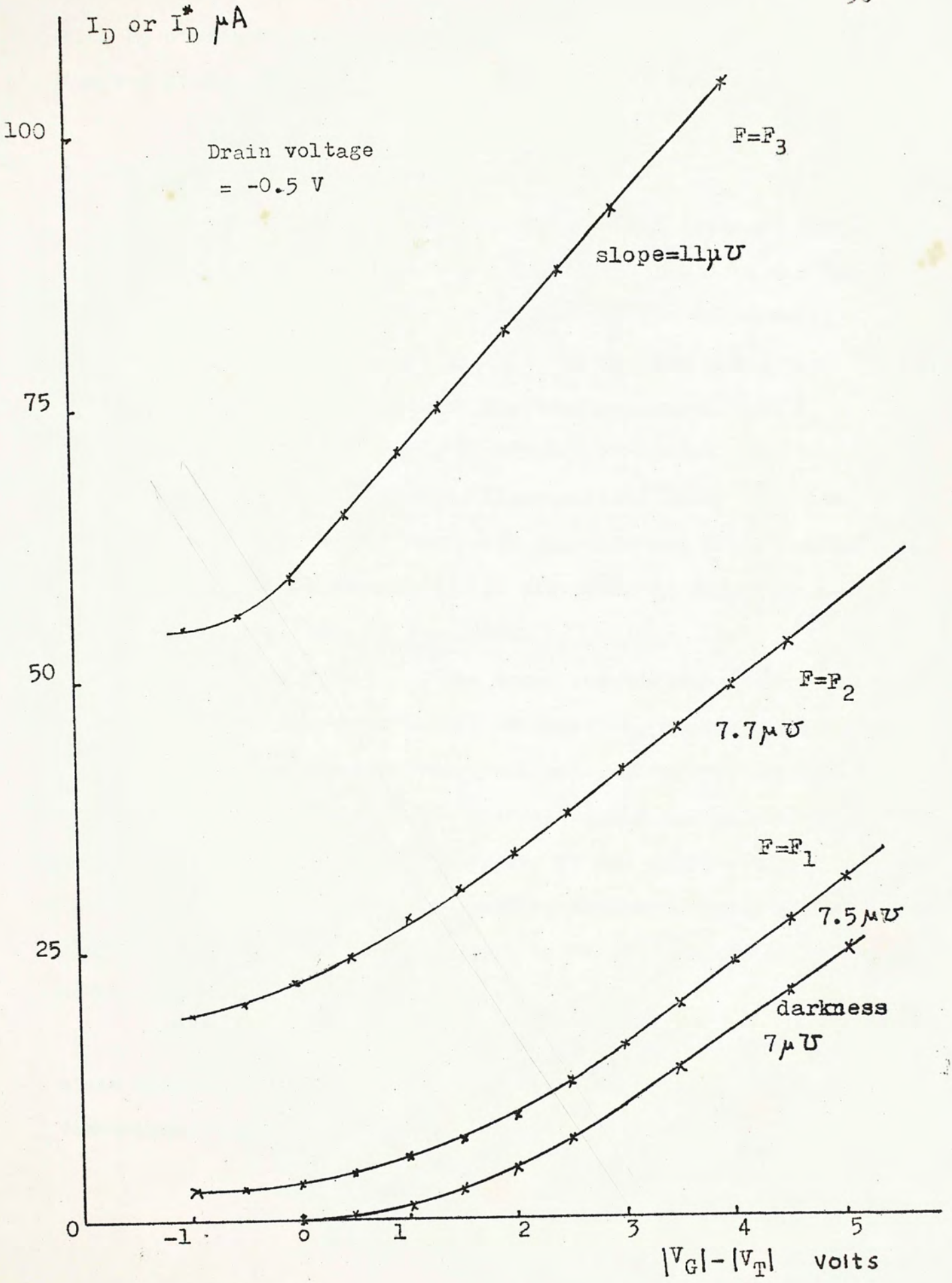
I_D or I_D^* μA
100
75
50
25
0
Drain voltage
= -0.5 V
F=F3
slope=11μυ
F=F2
7.7μυ
F=F1
7.5μυ
darkness
7μυ
-1
0
1
2
3
4
5
$|V_G| - |V_T|$ volts

Fig. 3.7

will be discussed to gain some insight into the mechanisms responsible for the photocurrent in the MOST.

3. 4a Photocurrent due to diffusion

It is observed that the photocurrent is constant for all gate voltages below a value of about $|V_T| - 1.5$ volt and that this photocurrent I_{po} is also independent of the drain voltage (Fig. 3.3- 3.6) I_{po} occurs when the Si surface under the gate oxide is in accumulation or flatband condition, and a channel has not been formed in darkness. It cannot come from the formation of a channel under illumination, since in that case the photocurrent will vary with the gate and drain voltages. However, it can be explained by the diffusion of photogenerated carriers in the Si bulk to the drain.

As shown in Fig. 3.8 (P.40), the drain and the substrate effectively form a reverse biased PN junction. Under accumulation, the surface charge layer is very thin and practically shields the bulk from the effect of the electric field due to the gate bias. The generated minority carriers in the substrate will move by diffusion towards the drain junction depletion region where they are swept by the electric field to the p-side of the junction, hence resulting in a photocurrent.

The diffusion current can be found by solving the steady state diffusion equation for the minority carriers. The one dimensional equation is used for simplicity.

$$D_p \frac{d^2 p}{dx^2} + G - \frac{p - p_o}{\tau} = 0 \qquad (3.1)$$

with the boundary conditions

$$p(\infty) = p_o + \tau G$$
$$p(0) = 0 \quad \text{for } V_D \gg \frac{kT}{q}$$

where D_p is the diffusion coefficient for holes

G optical generation rate of carriers

p_o bulk equilibrium hole concentration

τ lifetime of excess minority carriers

x distance measured in the substrate from the drain junction

Solution of Eq. 3.1 gives the diffusion current to be

$$A_J q D_p \frac{dp}{dx}\Big|_{x=0} = \frac{q D_p (p_o + \tau G)}{L_p} A_J \simeq \frac{q D_p \tau G A_J}{L_p} \qquad (3.2)$$

if $\tau G \gg p_o$

where A_J is the junction area normal to the current flow

L_p the diffusion length of holes

Eq. 3.2 can be interpreted as that the minority carriers generated within a diffusion length from the junction can reach the drain and result in a photocurrent. Provided the drain voltage is much greater than kT/q , this current is independent of V_D as observed.

Eq. 3.2 shows that the photocurrent I_{po} should be proportional to the optical generation rate and hence the light intensity. This is verified by the linear relationship between I_{po} and the light intensity F as shown in Fig. 3.9 .

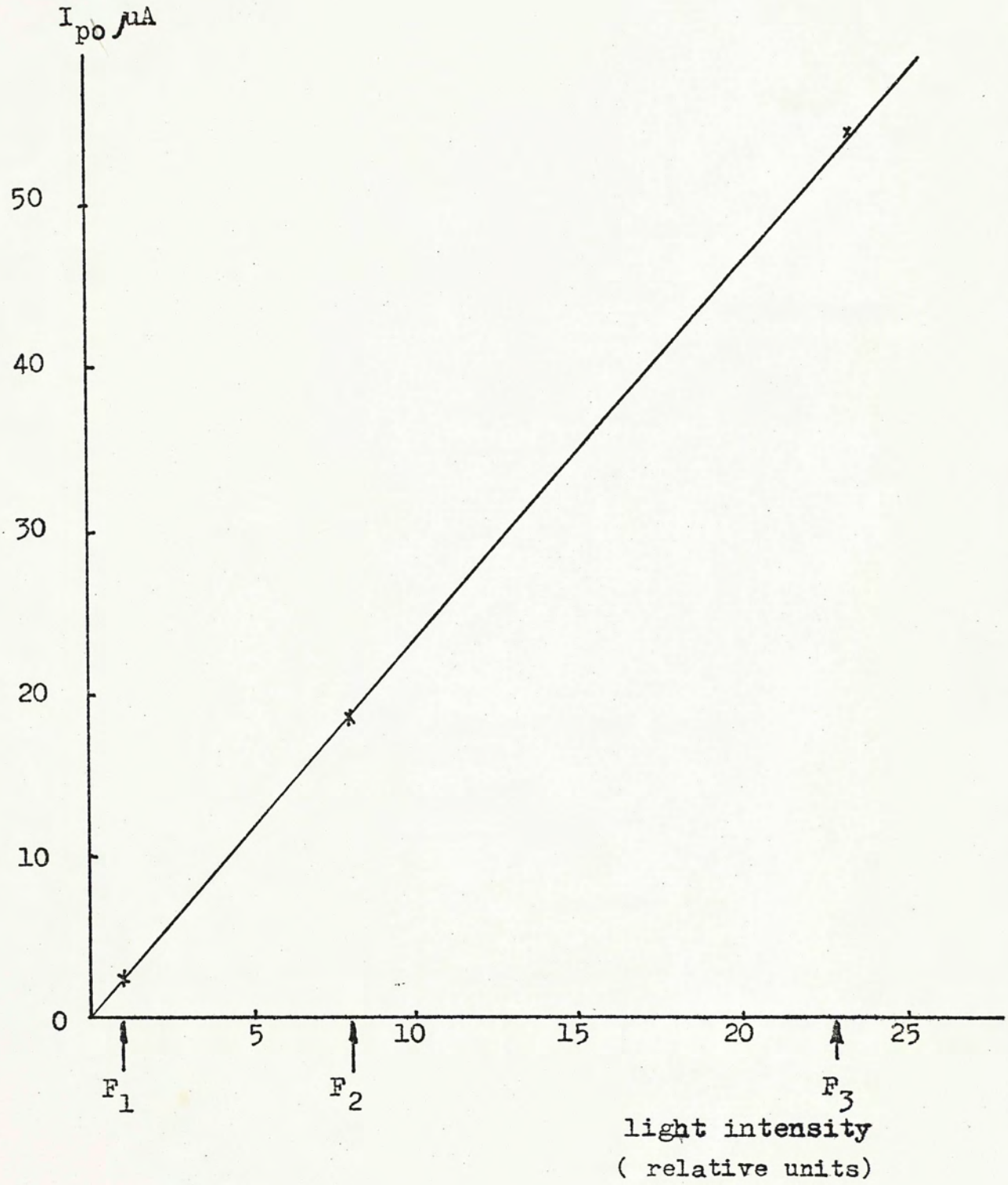
I_{po} μA
50
40
30
20
10
0
5
10
15
20
25
F_1
F_2
F_3
light intensity
(relative units)

Fig. 3.9

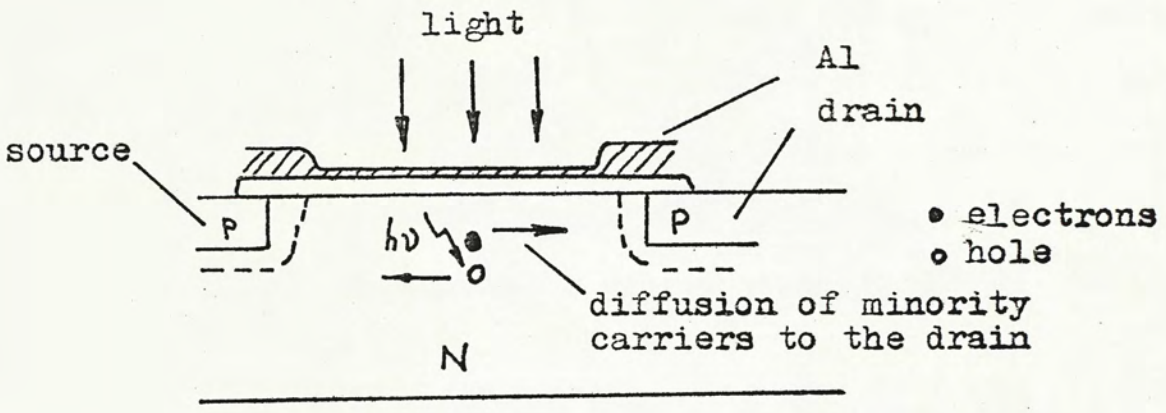

Fig. 3.8

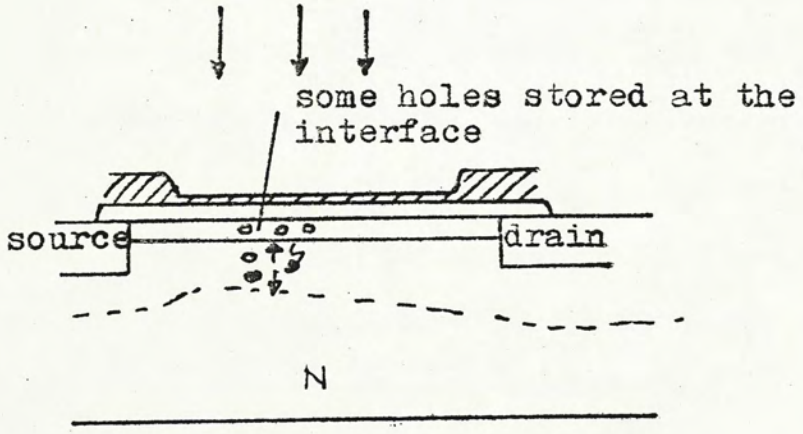

Fig. 3.10

3. 4b Photocurrent in the channel

It was found that the photocurrent started to rise from the above constant value as the gate voltage exceeded about $|V_T| - 1.5$ volts (Fig. 3.3). This fact suggests that there is a different mechanism responsible for the photocurrent. In this region, the photocurrent is a function of both the drain and gate voltages. It is thought that it comes from the increase of carrier concentration in the channel under illumination. Such a model, including the effect of trapping of excess carriers by the surface states, will be used to explain the dependence of the photocurrent on the bias voltages.

Consider the transient conditions in the MOST with an inverted channel when illumination is turned on. The drain voltage is so low that the channel is not pinched off. (fig. 3.10). The generated electrons and holes in the surface depletion region will be separated by the electric field present, with the result that the holes drift towards the channel, and the electrons towards the edge of the channel. Some of the holes are stored near the interface while others are drifted away by the electric field along the channel. The accumulation of excess holes near the interface hence increases the channel conductance.

The photocurrent was observed to increase at a gate voltage slightly less than the turn-on volatage $|V_T|$. It is because that the surface which is originally intrinsic or weakly inverted in darkness becomes strongly inverted due to charge injection under illumination, and a channel current flows.

The drain currents under illumination I_D^* as function of V_G at a drain voltage of -0.5 volt are shown in Fig. 3.7 together with I_D in darkness. (I_D^* is the sum of I_D and I_p

measured.) Before discussing I_D^*, we have to consider the effect of trapping of excess carriers in the channel by the surface states as revealed by the $I_D - V_G$ characteristics.

As discussed in chapter 1, the trapping of carriers in the channel by surface states results in a lower effective mobility. It has been shown that (from chapter 1)

$$I_D = \frac{Z}{L}\mu_p' C_i \left[(V_G - V_T)V_D - \frac{V_D^2}{2}\right] \qquad (3.3)$$

$$\therefore \frac{\partial I_D}{\partial V_G} = \frac{Z}{L}\mu_p' C_i V_D \qquad (3.4)$$

Therefore the slope of the graph of I_D as function of V_G is proportional to μ_p', and will be lower at small gate voltages if trapping of carriers by surface states exists. This effect is found to exist in our samples which probably have high surface state densities. The $I_D - V_G$ characteristic measured shows a bending at low $|V_G|$ just after the channel formation. At higher $|V_G|$, μ_p' is constant and I_D varies linearly with $|V_G|$.

The drain current I_D^* under illumination shows interesting differences compared with I_D in darkness. First of all, the variation of the slope $\frac{\partial I_D}{\partial V_G}$ is greatly reduced under illumination, especially at high light intensity. At light intensity $F = F_1$, F_2 there are still slight initial variation of $\frac{\partial I_D^*}{\partial V_G}$ followed by a constant slope at higher gate voltages; but at $F = F_3$, I_D varies linearly with V_G showing that no trapping of carriers by the surface states occurs. This can be explained by that the carrier concentration in the channel under illumination is

much greater than the charge trapped even at low gate voltages, and so there is little reduction in the effective hole mobility.

Another feature is that the drain current increases linearly with V_G in regions where no trapping by surface states are assumed to occur, but the transconductance defined by $\frac{\partial I_D^*}{\partial V_G}$ is different from $\frac{\partial I_D}{\partial V_G}$ in darkness. At strong illumination, $(F=F_3)$ the deviation between $\frac{\partial I_D^*}{\partial V_G}$ and $\frac{\partial I_D}{\partial V_G}$ may be significant. The increase of the transconductance under illumination means that on applying an increased electric field through the oxide, an increase of the hole concentration in the channel comes from both thermal and optical generation of carriers.

3, 4c Photocurrent after pinch-off of the channel

An increase of the drain voltage in general results in a higher electric field in the channel, and thus increases the conductance associated with the injected carriers in the channel as observed in the experiment. But the photocurrent reaches a plateau at a drain voltage which is found to correspond to the saturation drain voltage, and then decreases almost linearly as the drain voltage is increased beyond a certain value. (Figs. 3.4 , 3.5, 3.6). A constant value of I_p after pinch off is expected if we only consider the voltage across the channel to remain constant after pinch-off of the channel, and the drain voltage does not have any effect on the electric field in the channel. To give an explanation for the negative slope, we notice

that

$$I_D^* = I_D + I_p \qquad (35)$$

$$\frac{\partial I_D^*}{\partial V_D} = \frac{\partial I_D}{\partial V_D} + \frac{\partial I_p}{\partial V_D}$$

$\frac{\partial I_D}{\partial V_D}$ is positive in darkness representing a finite saturation drain conductance, but $\frac{\partial I_p}{\partial V_D}$ is found from experiment to be negative in the falling region of the graphs in Figs 3.4, 3.5, 3.6 . In fact, $\frac{\partial I_p}{\partial V_D}$, $\frac{\partial I_D}{\partial V_D}$ are found to have approximately the same order of magnitude. (table 3.1) This means that $\frac{\partial I_D^*}{\partial V_D}$ will be quite different from $\frac{\partial I_D}{\partial V_D}$.

Tab. 3.1

	g_{DS} (μv)	$\frac{\partial I_p}{\partial V_D}$ at linear deceasing region of I_p (μv)		
		F=F_1	F=F_2	F=F_3
$\lvert V_G\rvert - \lvert V_T\rvert$ = 2V	0.5	- 0.45	- 0.8	- 0.75
$\lvert V_G\rvert - \lvert V_T\rvert$ = 4V	1	- 0.8	- 1.3	- 1.25

It is suggested that the decrease of I_p at high $|V_D|$ is probably related to the current conduction mechanism after pinch-off of the channel, i.e. the effect of V_D on I_D by the channel length modulation and the drain-to-channel feedback can be quite different under illumination due to the presence of photogenerated carriers in the depletion region between the channel and the drain.

3. 5 Conclusion

In conclusion, the photocurrent of the MOST due to interband transition of carriers in the Si under the gate has been measured as functions of the drain voltage and the gate

voltage at different light intensity. It is shown that two mechanisms are responsible for the photocurrent observed: (1)diffusion of generated carriers in the bulk to the drain, (2) increase of hole concentration in the channel due to optical injection of charge. The transconductance and saturation drain conductance are found to be changed under illumination. The trapping effects of $Si-SiO_2$ interface states are discussed from the variation of the slope of the $I_D - V_G$ curve.

IV Direct excitation of interface state carriers by optical absorption in MOST

4.1 Introduction

In this chapter, the response of the semi-transparent gate MOST to monochromatic light with photon energy below the Si bandgap will be discussed. The main aim is to observe the possibility of exciting carriers at the $Si-SiO_2$ interface states directly by optical absorption to the energy bands by measuring the photocurrent. But experimental efforts have so far produced negative results. A simple theory of direct excitation of surface state carriers by photons will be derived, from which it is estimated that in Si a rathar high photon flux density is required to produce an observable effect, and that the light source used in the experiment will unlikely provide such a high intensity. As described in chapter 1, there were recent reports on using the surface photovoltage spectroscopy to study the surface state properties in some high bandgap semiconductors such as CdS, Ga As [17-20]. Some comparison between Si & CdS in the process of direct excitation of surface states will be made.

4.2 Experiment

Since the energy bandgap in Si is 1.1 eV, the wavelength

of the light used in our experiment will be in the infra-red range. Ordinary Tungsten lamps are not suitable since the glass envelope absorbs light of wavelength longer than 2μm. A globar with emission spectrum from 1μm to 10μm, and a Spex 1702 Spectrometer were used as the monochromatic light source. The experiment set up is shown in Fig. 4.1 .

All optics used in the spectrometer were mirrors and no lens were used. The amplification and detection of the photo-signal was the same as that described in chapter 3 using a Phase Sensitive Detector. A Si wafer was used as a filter to absorb light with photon energy greater than 1.1 eV due to the higher order lines from the diffraction grating. In the experiment, the filter was first moved so that visible light was incident on the sample, which was then aligned to achieve a maximum photocurrent detected.

No definite photocurrent as measured by the Phase Sensitive Detector output was observed under various bias conditions for light wavelength from 1.1μm to 3.2μm, (which correspond to photon energies from the bandgap to about 0.4 eV) including long term effect after illumination for a long time. Some theoretical considerations concerning the direct excitation of surface states in semiconductors will be given in the next section so as to gain some idea of the sensitivity of the experimental method used.

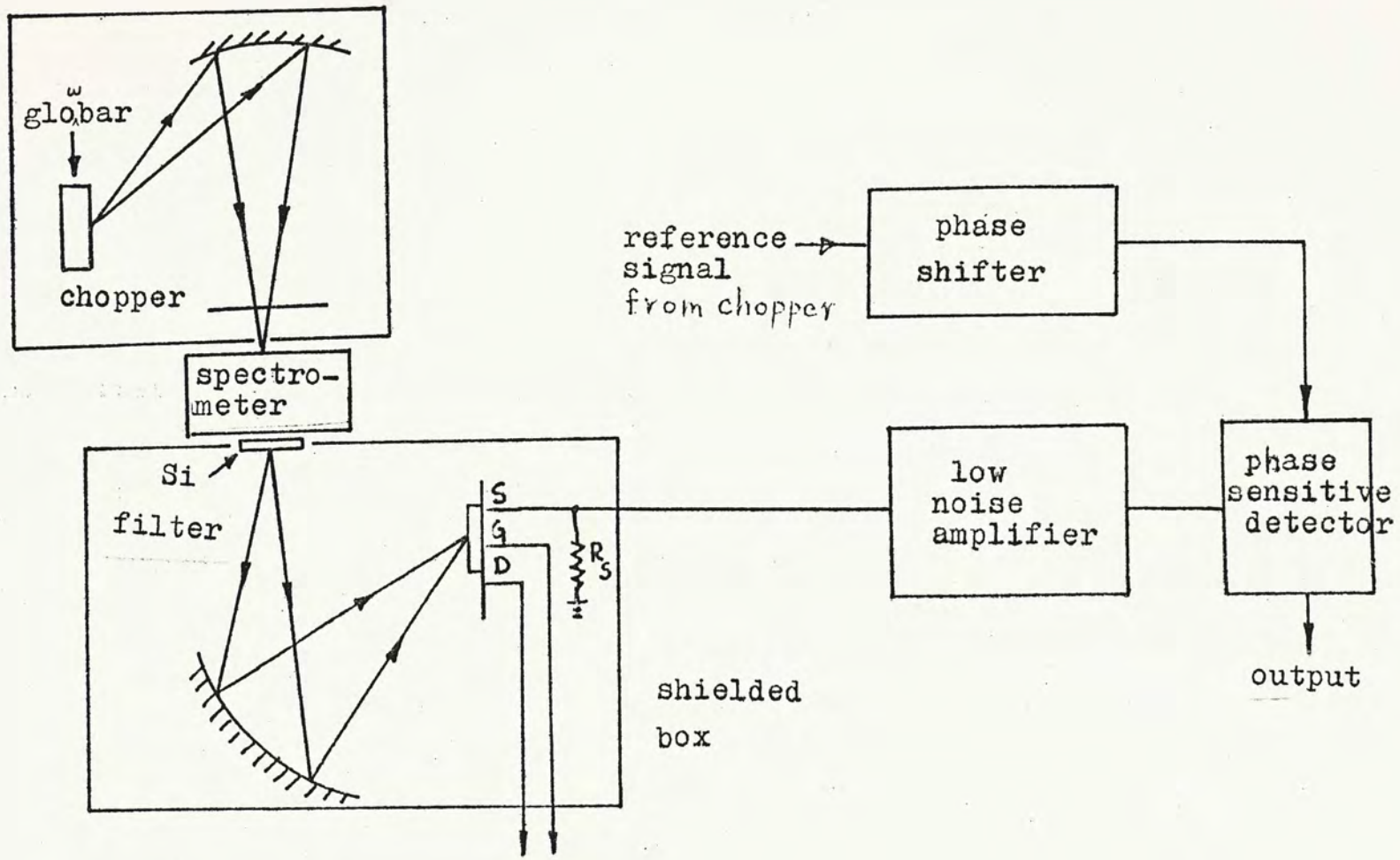

Fig. 4.1 Experimental set up for measuring the photocurrent in MOST due to direct excitation of surface states

4.3 Kinetics of direct excitation of surface state carriers by optical absorption

The kinetics of direct excitation of surface state carriers by photons will be considered from the dynamic equilibrium between the thermal and optical transition rates of carriers at the excited state. From this, the occupation probability by electrons at the surface state, and the resultant injection rate of carriers into the bulk are derived.

We shall consider the effect when only a single surface state is optically excited. Let us start with the dynamic equilibrium between a surface state and the energy bands by thermal transfer of carriers without any optical processes.[22] Four rates of flow are involved at the surface state, namely the thermal emission and capture of electrons and holes. If we apply sub-bandgap light of the appropriate photon energy, transition of carriers is induced between the surface state and the energy bands. In general, we have to consider six flow rates of carriers in establishing the steady state occupation probability by electrons at the surface state.

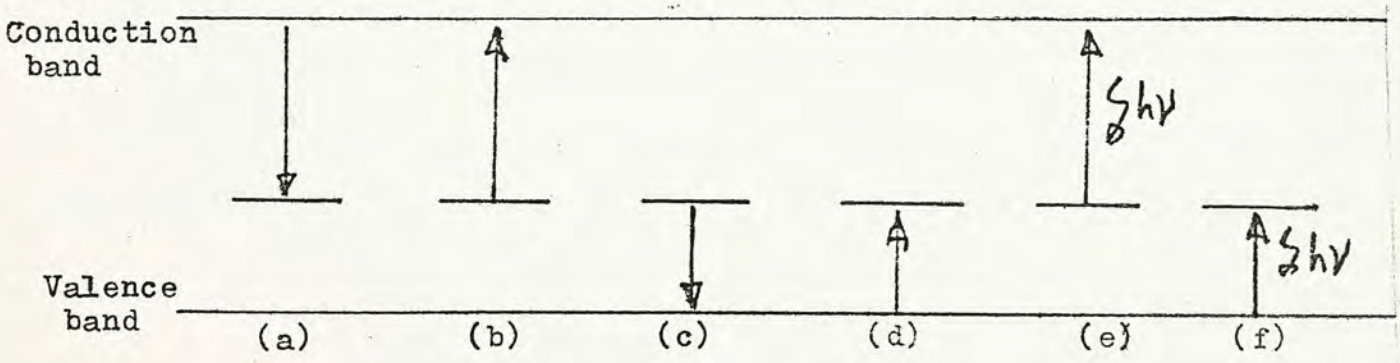

Fig. 4.2 Transition of carriers at the surface state
Arrows indicate directions of electron flow

Fig. 4.2 shows the simplified diagram indicating directions of electron flow between the conduction band, valence band and the surface state of energy level E_t. Radiative recombinations have been neglected.

Process (a) - thermal capture of electrons

Process (b) - thermal emission of electrons

Process (c) - thermal capture of holes

Process (d) - thermal emission of holes

Process (e) - optical emission of electrons

Process (f) - optical emission of holes

Rates of flow of carriers for the thermal capture and emission processes (a) to (d) are given by:[22]

$$\left.\begin{aligned} r_a &= c_n n_s^* N_t (1-f^*) \\ r_b &= e_n N_t f^* \\ r_c &= c_p p_s^* N_t f^* \\ r_d &= e_p N_t (1-f^*) \end{aligned}\right\} (4.1)$$

where N_t is the density of surface state (cm^{-2}) , f^* is the occupation probability by electrons at the surface state , n_s^* p_s^* are the electron and hole concentration at the surface under illumination. c_n , c_p are the thermal capture constants of electrons and holes at the surface state. They are usually expressed as:

$$c_n = v_{th}\sigma_n \qquad (4.1a)$$
$$c_p = v_{th}\sigma_p$$

where v_{th} is the thermal velocity of carriers and σ_n σ_p are the thermal capture cross section of electrons and holes.

e_n , e_p are the thermal emission constants of electrons and holes. Their relationship to c_n, c_p as derived from thermodynamic equilibrium conditions are:

$$e_n = c_n n_i \exp\left(\frac{E_t - E_i}{kT}\right) \qquad (4.1b)$$
$$e_p = c_p n_i \exp\left(\frac{E_i - E_t}{kT}\right)$$

Equs. 4.1 merely states the fact that the rate of thermal emission of electrons from the surface state is proportional to the density of electrons at the surface state, and the rate of thermal capture of electrons from the conduction band is proportional to the density of holes at the surface state and the electron concentration at the surface. Similar interpretation can be made of the thermal emission and capture of holes.

The optical excitation of electrons will occur if $h\nu \geq E_c - E_t$ and similarly for the optical excitation of holes if $h\nu \geq E_t - E_v$ The rates of photo-excitation should be proportional to the incident photon flux density F (cm^{-2} sec^{-1}) at the surface, and the density of carriers at the state excited, where the constant of proportionality has the dimension of area, and

is called the optical capture cross section of electrons or holes.

$$r_e = F\sigma_n^{\circ} f^* N_t$$
$$r_f = F\sigma_p^{\circ}(1-f^*) N_t \qquad (4.2)$$

where σ_n° is the optical capture cross section of electrons

σ_p° is the optical capture cross section of holes .

It should be noted that the optical capture cross sections defined above really represent the transition probabilities of electrons between the surface state and energy bands by photon absorption as determined by quantum mechanical calculations.

At steady state, the concentration of electrons at the surface state remains constant, i.e.

$$r_b + r_e - r_a = r_d + r_f - r_c \qquad (4.3)$$

The solution of Eq. 4.3 after substituing the values of r_a, r_b, r_c, r_d, r_e, r_f gives

$$f^* = \frac{c_n n_s^* + e_p + F\sigma_p^{\circ}}{c_p p_s^* + c_n n_s^* + e_n + e_p + F(\sigma_n^{\circ} + \sigma_p^{\circ})} \qquad (4.4)$$

The net rate of electrons flowing from the surface state to the conduction band as given by $(r_b + r_e - r_a)$ may not be necessarily zero. Thus there is an injection of electrons and holes into the bulk under excitation of surface state carriers. The rate of injection G_s^* (cm^{-2} sec^{-1}) as given by $r_b + r_e - r_a$ can be expressed by the following equation after eliminating f^* from Eq. 4.4

$$G_s^* = N_t \left[\frac{c_n c_p (n_i^2 - n_s^* p_s^*) + F(\sigma_n^\circ e_p + \sigma_p^\circ e_n) + F^2 \sigma_n^\circ \sigma_p^\circ}{c_p p_s^* + c_n n_s^* + e_n + e_p + F(\sigma_n^\circ + \sigma_p^\circ)} \right] \quad (4.5)$$

It should be noted that in darkness when $\sigma_n^\circ = \sigma_p^\circ = 0$, f^* in Eq. 4.4 reduces to the normal Fermi-Dirac occupation probability, and G_s in Eq. 4.5 reduces to the surface thermal generation rate.

4.4 Photocurrent in the MOST due to direct excitation of Si-SiO_2 state carriers by photons:

There are two ways by which direct excitation of surface state carriers can contribute to a photocurrent in the MOST. It is shown in the previous section that the occupation probability at the surface state is changed, and there is a steady state injection of electrons and holes into the semiconductor. These effects at different photon energies are described below:

A. With photons of energy less than half the bandgap:

As shown in Fig. 4.3 , in a n-type bulk, photons of the appropriate energy less than half the bandgap will only induce transitions of holes from the surface states near the Fermi-level (E_{FP}) to the valence band. Consequently the negative charge at the excited surface states will be increased. If we assume that the excited holes stay in the inverted layer, the channel conductance will be increased.

The steady state injection of carriers into the channel

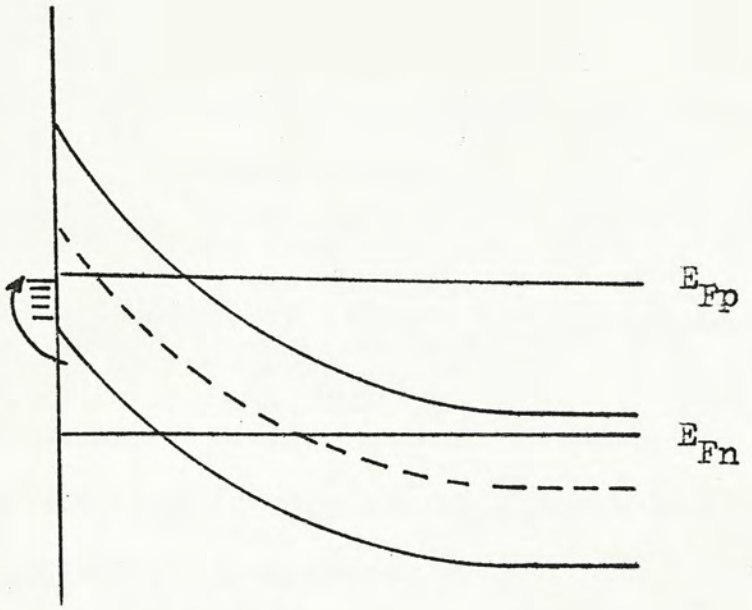

Fig. 4.3 Energy band diagram of a P-channel MOST with only holes excited from the surface states near the fermi level to the valence band

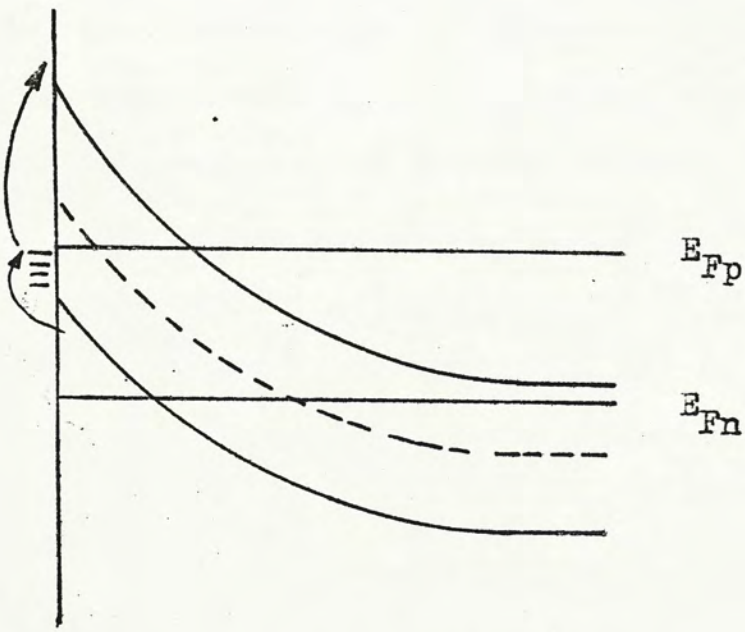

Fig. 4.4 Energy band diagram of a P-channel MOST with both electrons and holes excited from the surface states near the fermi level to the energy bands

will be negligible with only holes excited by the photons, since the rate of electrons entering the conduction band is limited by the low thermal emission rate of electrons from states situated below the mid-gap. This can be seen from Eq. 4.5 where if $\sigma_n^\circ = 0$, G_s^* mainly comes from the term $F\sigma_p^\circ e_n$. So a low emission constant e_n directly reduces the rate G_s^*.

B. With photons of energy greater than half bandgap:

As shown in Fig. 4.4 , there are in general transitions of both electrons and holes from the surface states near the Fermi level E_{FP} to the energy bands. Since both positive and negative charges are excited from the surface state, the net change in the charge will not be significant. So we expect the photo-conductance coming from the increase of holes in the channel to be small. This condition corresponds to the quenching of surface photovoltage as measured in CdS [20]. Eq. 4.4 shows that the change in f is small compared with the case where only one type of carrier is excited, because both the numerator and denominator are increased by $F\sigma_p^\circ$ and $F(\sigma_n^\circ + \sigma_p^\circ)$ respectively in the expression for f^* .

The injection of carriers into the channel may be however important because electrons in the surface state can be excited to the conduction band followed by a thermal or optical emission of holes from the surface state to the valence band.

4.5 Estimation of the Sensitivity of the experimental method:

Since there is no reported value for the capture cross section of photons at the Si-SiO_2 interface states, the following estimation is merely based on an assumed value of $\sigma_n^\circ = \sigma_p^\circ = 10^{-17} cm^2$ similar to that measured in CdS [19].

Suppose the MOST is biased so that a channel is just formed and is far from pinch-off. If photons of appropriate energy less than half the bandgap is applied, holes are excited from a small range of surface states near the Fermi level E_{FP} to the valence band. We shall use eqn. 4.4 to calculate the change in the occupation probability by electrons (Δf) at the excited state. It is assumed that the charge transfer between the surface state is small so that the surface carrier concentration is not affected. For an inverted p-channel, the surface electron concentration is much lower than that of holes, so that the thermal capture of electrons from the conduction band as represented by the term $c_n n_s$ can be neglected. Under this assumption, Equation 4.4 gives

$$\Delta f = \frac{e_p + F\sigma_p^\circ}{c_p p_s + e_n + e_p + F\sigma_p^\circ} - \frac{e_p}{c_p p_s + e_n + e_p}$$

$$= \frac{F\sigma_p^\circ (e_n + c_p p_s)}{(c_p p_s + e_n + e_p + F\sigma_p^\circ)(e_n + e_p + c_p p_s)} \qquad (4.6)$$

We shall calculate the surface hole concentration per unit area when the channel is just turned on by the formula $I_D = q\mu_p' Z Q_p V_D / L$ which is obtained if the drain voltage is much lower than $|V_G| - |V_T|$. For our sample, $Q_p \sim 10^{10}$ cm^{-2} at $V_D \sim 0.5V$ corresponding to a drain current of 1μA. It is estimated that our Phase Sensitive Detector system can measure a fractional change of about 10^{-3} in the drain current, i.e. a hole density of about 10^7 cm^{-2}.

Since the increase of channel charge is equal to the change in surface state charge, Δf is of the order of 10^{-3} for a typical value of $N_t = 10^{10}$ cm^{-2}. Substituting the values of $\sigma_p^\circ = 10^{-17}$ cm^2, $e_n = 4.56 \times 10^{-2}$ sec^{-1}, $e_p = 2.8 \times 10^2$ sec^{-1} $c_p p_s = 10^4$ sec^{-1} for a state of 0.4 eV above the valence band in Eq 4.6 shows that the photon flux density is of the order of 10^{18} cm^{-2} sec^{-1}. (The thermal capture cross sections are estimated from data in Ref. 14)

Let us consider the generation current obtained when both electrons and holes are excited from the set of surface states mentioned above by photons of energy greater than half the bandgap. If we use the same photon flux density of $F = 10^{18}$ cm^{-2}sec^{-1} substitution of the parameters in Eqn. 4.5 indicates that the photocurrent I_p resulting from an increase of the injection G_s is only about 5×10^{-12} A for our sample. $\{ I_p = q Z L (G_s^* - G_s) \}$ It is because that at this photon flux density, the optical generation rate of carriers is even much less than the

original thermal generation rate. So it is concluded that a photocurrent by this process requires even higher photon flux density, and the value of $F = 10^{18}$ cm^{-2} sec^{-1} is the minimum estimated value for an observable photocurrent.

A glo$\overset{\omega}{\wedge}$bar operates at a temperature of about 1500^{o} K, and has an emissitivity of approximately 0.8 in the range from 1.5μm to 15μm. Assuming Planck's Law of black body radiation, we may estimate from these data a value of about 10^{18} cm^{-2} sec^{-1} for the photon flux density radiated in the frequency range 0.4 ± 0.05 eV. But we have to include a loss factor since only a fraction of the total radiated energy is collected by the optics used. From the solid angle subtended by the mirror at the light source, this factor is about 10^{-3}. So the photon flux density reaching our sample is only of the order of 10^{15} cm^{-2} sec^{-1}, and is unlikely to meet the sensitivity requirement of our experiment.

4.6 Comparison between Si and CdS in the process of direct excitation of surface states

It seems appropriate here to point out some reasons for the difficulty of observing the effects of direct excitation of surface states in Si compared with other high bandgap semiconductors such as CdS, where significant surface photovoltage

can be observed even with sub-bandgap light. First of all, the light wavelength required in Si is in the infrared region, and it is difficult to find suitable powerful light source at these wavelengths. Besides, another factor reduces the sensitivity of experimental observation in Si even for the same surface state density, optical capture cross section and incident photon flux density. It is because while the surface states in Si are in good communication with the bulk, the rates of exchange of carriers between the surface states and the energy bands are very low in CdS. In fact, the CdS surface states may not be in equilibrium with the bulk for several years due to the low capture cross section for electrons at the surface states (about 10^{-18} cm^2) and the low surface carrier concentration. (19) The surface barrier for a n-type CdS of resistivity of 1 ohm-cm was measured to be 0.5 V from which a surface concentration of electrons of 10^6 cm^{-3} can be calculated. We may compare these values with the intrinsic carrier concentration of 1.6×10^{10} cm^{-3} and the thermal capture cross section of 10^{-15} cm^2 in Si .

Eq. 4.6 indicates that the value of Δf is very much dependent on the relative magnitudes of $F \sigma_p^0$ and $(e_n + e_p + c_p p_s)$. If the photo-excitation term is much larger than the thermal emission and capture of carriers, Δf approaches $\frac{e_n + c_p p_s}{e_n + e_p + c_p p_s}$; but otherwise Δf is small. (The expression for f is not exactly valid for CdS, since it assumes a thermal equilibrium

occupation probability in darkness, but it still illustrates the effectiveness of the change of surface state charge by photon absorption.)

The physical meaning is that if the communication between the surface states and the energy band by thermal processes is so good that the change in charge at the surface state due to photon absorption is balanced by the adjustments of thermal transition of carriers, the overall effect of Δf is small. The converse is true when the surface states are in poor communication with the bulk since the rate of re-capture of excited charge by the surface states will be low.

Since the thermal transition rates of carriers in Si are many orders of magnitude higher than that in CdS, the effects of direct excitation of surface states would be more difficult to be observed. Low temperature measurement may improve the sensitivity since it reduces the surface carrier concentration and hence the communication between the surface states and the bulk.

4.7 Conclusion

The result of observing the photocurrent in the MOST due to direct optical absorption by the Si-SiO_2 interface states was so far negative with the available infrared source. A simple theory concerned with the kinetics of thermal and optical rates at the surface state was used to estimate the photon

flux density required for a detectable effect. It can be shown that in semiconductors where the surface states are not in good thermal communication with the bulk, optical absorption by surface states results in more significant change in the surface state charges. In experiments with Si surfaces, a powerful infrared source (tunable laser) and low temperature should be considered for improving the sensitivity.

Appendix

We shall describe here a method to measure the relative flux densities F of photons with energy greater than the Si bandgap reaching the sample at different light bulb voltages. Its principle is based on the measurement of the surface photovoltage in an MOS capacitor biased in strong inversion.[14] It can be shown that the surface photovoltage Δu_s of a MOS capacitor in the inversion region satisfies (for n-type bulk)

$$\lambda^{-2} \exp(\Delta u_s) + 1 + \Delta_p - \frac{\partial \Delta_p}{\partial \Delta u_s} = 0 \qquad (A.1)$$

where the doping factor λ and injection factor Δ_p are as defined in Equation 1.15.

In strong inversion, equation A.1 reduces to a simple form since $\lambda^{-2} \exp(\Delta u_s) \ll 1$,

$$\Delta u_s = \ln(1 + \Delta_p) \qquad (A.2)$$

Thus the injection factor $\Delta_p = \frac{\Delta p_o}{p_o}$ can be obtained from the value of Δu_s in equation A.2. Since Δ_p is proportional to the flux density of photons causing interband transition, measurement of Δu_s of the MOS capacitor in strong inversion gives the relative light intensity reaching the sample at different light bulb voltages.

For measurement of the surface photovoltage, the source and drain of the MOST were open circuited. Bias to the gate was applied through a 10^8 resistor. The potential across the gate was picked up by an electrometer before fed to the low noise amplifier. The rest of the phase sensitive detector system was the same as that described in chapter 3.

References

1. W. Shockley, G.L. Pearson
   Modulation of Conductance of Thin Films of Semiconductors by Surface Charges
   Phys. Rev., 74, 232 (1948)
2. H.K.J. Ihantola, J.L. Moll
   Design Theory of a Surface Field Effect Transistor
   Solid State Electron., 7, 423 (1964)
3. C.T. Sah
   Characteristics of the Metal-Oxide-Semiconductor Transistor
   IEEE Trans. Electron Devices, ED-11, 324 (1964)
4. S.R. Hofstein, F.P. Heiman
   The Silicon-Insulated-Gate Field Effect Transistor
   Proc. IEEE, 51, 1190 (1963)
5. Paul Richman
   Characteristics and Operation of MOS Field-Effect Devices
   Chapter 2
   McGraw Hill Book Company, 1971
6. J.R. Schrieffer
   Effective Carrier Mobility in Surface-space Charge Layers
   Phys. Rev., 97, 641 (1955)
7. S.R. Hofstein, G. Warfield
   Carrier Mobility and Current Saturation in the MOS Transistor
   IEEE Trans. Electron Devices, ED-12, 129 (1965)

8. V.G.K. Reddi, C.T.Sah

Source to Drain Resistance Beyond Pinch-off in Metal-Oxide-Semiconductor Transistors

IEEE Trans. Electron Devices, ED-12, 139 (1965)

9. Garett, Brattain

Physical theory of semiconductor surfaces

Phys. Rev. 99, 376 (1955)

10. E.O. Johnson

Large signal surface-photovoltage studies with Ge

Phys. Rev. 111, 153 (1958)

11. R. Williams,

Surface Photovoltage Measurements on CdS

J. Phys. Chem Solids 23, 105 (1962)

12. H. Yamagishi

Fermi level stabilisation and surface states at the interface of Si (111) surfaces and insulating layers

J. Phys. Soc. (Japan) 25, 766 (1968)

13. Y.W. Lam,

Surface State density and surface potential in MIS capacitors by SPV measurements I

J.Phys. D Appl. Phys. Vol 4 , 1370 (1971)

14. Y.W. Lam, E.H. Rhoderick

Surface state density and surface potential in MIS capacitors by SPV measurements II

J.Phys. D Appl. Phys. Vol 4 , 1376 (1971)

15. M.S. Mock

A 2-dimensional Mathematical Model of the IGFET

Solid State Electron, 16, 601 (1973)

16. D. Vandrope

An accurate 2-dimensional Numerical Analysis of the MOS Transistor

Solid State Electron, 15, 547 (1972)

17. C.L. Balestra, J. Lagowski, H.C. Gatos

Determination of surface state energy positions by Surface Photovoltage Spectrometry: CdS

Surface Sci. 26, 317 (1971)

18. C.L. Balestra, J. Lagowski, H.C. Gatos

Photovoltage Inversion Effect and its application to Semiconductor Surface Studies

Surface Sci. 27, 547 (1971)

19. C.L. Balestra, J. Lagowski, H.C. Gatos

Determination of Surface state Parameters from Surface Photovoltage Transients in CdS

Surface Sci. 29, 203 (1972)

20. C.L. Balestra, J. Lagowski, H.C. Gatos

Electronic Characteristics of "Real" CdS surfaces

Surface Sci. 29, 213 (1972)

21. C.L. Balestra, J. Lagowski, H.C. Gatos

Surface Photovoltage Spectroscopy and Piezeelectric Effect in Ga As

Surface Sci. 40 , 216 (1973)

22. W. Shockley, W.T. Read

Statistics of the Recombination of Holes and Electrons

Phys. Rev., 87, 835 (1952)